UNIVERSITY OF OKLAHOMA
GRADUATE COLLEGE

GIANT GRAINS IN THE AKIYOSHI LIMESTONE: A RECORD OF ATMOSPHERIC CIRCULATION OVER THE PANTHALASSIC OCEAN

A THESIS
SUBMITTED TO THE GRADUATE FACULTY
In partial fulfillment of the requirements for the
Degree of
MASTER OF SCIENCE

By

PATRICK R. KELLY
Norman, Oklahoma
2021

GIANT GRAINS IN THE AKIYOSHI LIMESTONE: A RECORD OF ATMOSPHERIC CIRCULATION OVER THE PANTHALASSIC OCEAN

A THESIS APPROVED FOR THE
SCHOOL OF GEOSCIENCES

BY THE COMMITTEE CONSISTING OF

Dr. Gerilyn S. Soreghan, chair

Dr. Michael J. Soreghan

Dr. Shannon A. Dulin

Dr. Nicholas G. Heavens

Dr. Lindsey E. Hunt

Acknowledgements

This research was supported by the National Science Foundation (EAR-0745961 and EAR-1338331 to G.S. Soreghan, and EAR-1338440 to the University of Michigan). Supplementary funding was provided by the Eberly Family Chair (University of Oklahoma). Without funding from these sources, none of this work would have possible, so thank you for supporting this project. Thanking you to my advisor, Dr. Gerilyn Soreghan and my graduate committee comprised of Dr. Michael Soreghan, Dr. Shannon Dulin, Dr. Nicholas Heavens, and Dr. Lindsey Hunt for their unwavering assistance and vast knowledge in the variety of topics breached in this work. Thank you to Dr. Hiroyoshi Sano for essential guidance and collaboration in the field collections and geological expertise in the Akiyoshi terrane, as well as Dr. Vladimir Davydov for his work on fusulinid biostratigraphy for Moscovian — Asselian aged strata, and Dr. Katsumi Ueno for their help with Sakimarian and Artinskian fusulinid biostratigraphy for the Akiyoshi Limestone. Thank you to Dr. James Gleason for his assistance in understanding the Nd-Sr isotopic analyses that were obtained from the University of Michigan, Department of Earth and Environmental Sciences. Thank you to everyone who worked on the Akiyoshi samples prior to me, especially electron microprobe operator George Morgan, SEM operator Dr. Preston Larson, and prior master's students Xiao Qi and Elisheva Patterson. Lastly, thank you to the family and friends that have provided me with their seemingly endless support throughout the completion of this thesis.

Table of Contents

List of Figures

List of Tables

List of Appendices

Abstract

Models indicate that atmospheric transport distances for large windblown particles are limited to tens to perhaps hundreds of km owing to rapid gravitational settling, yet a number of studies of modern–recent sediment have documented the enigmatic transport of so-called “giant” (generally >63 μm) grains over thousands of km. Additionally, stratospheric injection of tephra by volcanic eruptions has the potential to increase the atmospheric transport distance of volcanically sourced material in particular. Here we report the first finding of giant grains in Earth’s pre-Pleistocene record, within upper Carboniferous–Permian shallow-marine carbonates of the Akiyoshi (paleo)atoll, which formed in the vast equatorial Panthalassic ocean. Grains with diameters commonly ~300 μm and up to ~2 cm occur, transported at least 4,500 km and up to 14,000 km away from the nearest viable source regions. Textural and compositional (both mineralogical and geochemical) data indicate the presence of both continentally sourced eolian grains and volcanically sourced grains, with the relative proportions of volcanic to continental grains peaking in the Moscovian (middle Late Carboniferous). The timing of volcanic versus continental grain deposition indicates that large-magnitude volcanic eruptions affected this part of equatorial Panthalassa in the Late Carboniferous, and that Pangaean continental aridity significantly increased into the Permian. Compositional data indicate likely source regions west of the Akiyoshi atoll, consistent with the common occurrence of westerlies over this equatorial region, thus indicating the operation of monsoonal circulation over the Paleo-Tethys sea.

Introduction

Mineral aerosols (dust) are an important component of the atmosphere, affecting both direct and indirect radiative forcing, as well as ecosystem fertilization, and cloud formation (e.g., Boyd et al., 2000; Mahowald and Kiehl, 2003; Kardys et al., 2011). Most research on dust focuses on the fine (< 20μm) component, as fines can remain suspended for long distances, whereas models suggest that coarse particles rapidly settle proximal to their source(s) (Mahowald, 2011; Adebiyi and Kok, 2019). In the last few decades, however, observations from atmospheric sampling and recent sediment deposits have found evidence for surprisingly long-range transport of so-called "giant" grains (>63 μm) (Betzer et al., 1988; Hayasaka et al., 1990; Ram and Gayley, 1991; Van Maldern et al., 1992; Arimoto et al., 1997; Middleton et al., 2001; Van der Does et al. 2018; Ryder et al., 2019; Varga et al. 2021). Documentation of the prevalence of this phenomenon through time is important since coarse grains affect climate differently than fines. Coarse particles can increase absorption of incoming and outgoing solar radiation, promoting warming, and increase cloud cover owing to their enhanced capability as cloud condensation nuclei (CCN) (Boyd et al., 2000; Nenes et al., 2014; Kok et al., 2017; Adebiyi and Kok, 2019). Currently, the climate effects of coarse grains are mostly neglected in models due to the short anticipated residence times of such grains.

In addition to their effects on climate, coarse grains can act as a tracer of atmospheric circulation as well as a proxy for the relative moisture of source regions, and – potentially—the prevalence and explosivity of volcanism. Accordingly, giant grains offer a potential trove of paleoclimatic data previously undocumented in the geologic record.

In this study we present the first analysis example of extreme, long-range transport of giant grains in Earth's deep-time record, specifically within the Carboniferous-Permian Akiyoshi Limestone (Japan), which formed part of an atoll in the Panthalassic Ocean. The giant grains preserved here capture transport from both explosive volcanic and arid continental sources. These data shed light on volcanic events and

climatic conditions during the study interval and demonstrate the ubiquity of the atmospheric transport of giant grains, even in Earth's deep-time record.

Geologic Background

Depositional and Tectonic Setting of the Akiyoshi Terrane

The Akiyoshi Terrane of southwest Japan (Fig. 1; Appendix 1) is an accretionary complex comprising oceanic and trench-fill deposits of Carboniferous to Permian age (Kanmera and Nishi, 1983; Kanmera et. al., 1990; Sano and Kanmera, 1991). The Akiyoshi Limestone rests on a basaltic seamount that formed within the equatorial Panthalassic ocean (Fujiwara, 1971; Sano and Kanmera, 1988). The Akiyoshi Limestone, a shallow marine unit that accumulated atop the atoll, together with basinal- deep marine chert, formed in an oceanic setting from middle Viséan to late Guadalupian time (Sano and Kanmera, 1988; Sano and Kanmera, 1991). The Akiyoshi atoll neared and was ultimately obducted onto the Japan margin in the late Permian (Kanmera et. al., 1990; Sano and Kanmera, 1991; Kasuya et al., 2012).

Post-Paleozoic remagnetization of the Akiyoshi Limestone precludes precise paleolatitudinal reconstructions (Moringa et al., 1988), but recent analyses of the analogous (coeval paleoatoll terrane) limestone in Kyushu, south of the Akiyoshi Terrane, yielded a weak primary magnetic remanence indicating a paleolatitude of ~12°S (Kirschvink et al., 2015), consistent with Kasuya et al.'s (2011) placement of the Akiyoshi Limestone at a position of ~15°N (~260 Ma). The Gplates reconstruction by Domeier and Torsvik (2014) indicates generally northward plate motions through the time of deposition of the Akiyoshi Limestone, implying the Akiyoshi atoll was positioned at latitudes ~10°N or lower from Middle Pennsylvanian through Early Permian time. Using two plausible end-member assumptions for plate velocity, 5 cm/yr and 10 cm/yr, chosen because larger oceanic plates tend to display higher spreading rates related to enhanced slab pull of oceanic lithosphere (Muller et al, 2008), the Akiyoshi

Terrane likely moved ~1,250 km – 2,500 km between the Moscovian and Artinskian Stages. The location of the Akiyoshi Terrane is unaffected by the ongoing controversy between the Pangaea A and Pangaea B reconstructions, but these reconstructions do imply different distances of the Akiyoshi Terrane from potential sources of volcanic and arid continental material (Kent and Muttoni, 2020) (Figure 1), as addressed further below.

Paleoclimatic Setting

The Late Paleozoic Ice Age (LPIA) was a time of intense global cooling beginning in the late Devonian and persisting to Middle–Late Permian time, with glaciation varying in intensity and spatial distribution throughout (e.g., Isbell et al., 2003, Fielding et al., 2008; Montañez and Poulsen, 2013; Soreghan et al., 2019). Widespread evidence for continental glaciation that grounded to sea level exists across many of the Gondwanan continents of the southern paleo-pole (e.g. Isbell et al., 2003; Fielding et al., 2008a,); additionally, controversial evidence exists for upland glaciation in western and eastern equatorial Pangaea (e.g. Becq-Giraudon et al., 1996; Soreghan et al., 2008, 2014; Pfeifer et al., 2020). As measured by the extent of diamictite distribution, glaciation peaked in the Asselian (earliest Permian) and largely collapsed by the Artinskian (e.g., Montañez and Poulsen, 2013; Soreghan et al., 2019); widespread exposure of epeiric systems near the time of the Carboniferous-Permian boundary corroborates the glacial maximum potentially occuring at this time (Koch et al., 2011), although fusulinid data suggest the maximum fell in Late Asselian — Early Sakmarian (Davydov et al., 2013). Far-field (low-latitude) records of the LPIA include carbonate-dominated cyclothems in Laurentia, recording glacial-interglacial eustatic variations (e.g., Heckel, 1993; Bishop et al., 2010). Shallow-marine carbonate strata of the oceanic Akiyoshi Limestone similarly record sea-level variations inferred to reflect glacioeustasy (Nakazawa and Ueno, 2004; Sano et al., 2006).

Methods

Several discrete intervals (10–20 m) of the Akiyoshi Limestone representing the mid-Moscovian (21 m), latest Kasimovian–early Gzhelian (13 m), latest Asselian (3.5 m)–earliest Sakmarian (12 m – 20 m), and late Artinskian times (70 m in total) were logged and sampled at 20 cm increments (Figure 2) (see Patterson, 2011 and Qi, 2016). A disconformity discovered in the upper Asselian-lower Sakmarian section resulted in a truncated Asselian interval of only 3.5 m. Fusulinoidean biostratigraphy (by Dr. V. Davydov for Moscovian — Asselian strata and K. Ueno for Sakimarian — Artinskian) provided age constraints. Here, we focus specifically on the "giant" grains (operationally defined here as grains with long axes generally larger than silt size (> 63 μm) recovered both in previous work (Patterson, 2011; Qi, 2016), and in newly processed sections. For both previously collected and new sections, thin section analyses guided facies and stratigraphic analyses, as well as fusulinid determinations.

For all samples, detrital silicate minerals, interpreted as atmospheric dust, were extracted following the procedure in Sur et al. (2010). Briefly, samples were cleaned of external debris by washing with 1N HCl, rinsed with distilled water, then dried, crushed to pea size, and rinsed again. Approximately 200–300 g of the resultant gravel was weighed, then subjected to dissolution in 2N HCl at 50˚C. The insoluble residue was then rinsed and centrifuged several times with distilled water, freeze dried, weighed, then combusted at 550˚C for 24 hours to remove organic matter and oxidize any pyrite. Subsequently, iron oxides were removed using citrate-bicarbonate-dithionite (CBD) followed by rinsing and freeze drying to obtain the final mass of the silicate mineral fraction (SMF).

A selection of the largest grains (n=1-30/sample), as well as a random sampling (up to 70) of additional grains were analyzed with respect to their shape, surface textures, and compositions using backscattered-electron (BSE) imaging using a scanning electron microscope (SEM) and electron microprobe (EPMA). Randomization was done by numbering the grains and using a random number generator for grain selection. For samples yielding < 10 giant grains, all grains were mounted for analysis. Grain dimensions (short- and long axes), qualitative shape (angularity), and elemental composition (for

mineralogy) were determined using back-scattered electron (BSE) and energy dispersive x-ray spectroscopy (EDXS) modes. Authigenic quartz grains, identifiable by their prismatic shape, were included in the random sampling, however, this was to measure the ratio of authigenic to detrital grains within each section. Authigenic grains were not considered during the remainder of this study.

Results—Grain Textures and Compositions

Of 283 limestone samples processed, 80 (~28%) yielded giant grains. Most of the giant grains retrieved from the Akiyoshi Limestone fall within the sand fraction, up to 2 mm in diameter (very coarse sand); however, nine igneous lithic fragments from three discrete horizons (levels 3.9, 4.9, and 16.7 m from the base of the section) of the Moscovian interval exceeded sand size, measuring from 2 mm–2 cm diameter in long dimension (figure 3). Excluding these nine lithic fragments the average giant grain exhibits a long axis of 257 μm and a short axis of 186 μm. Table 1 summarizes average and maximum sizes for each time slice.

Of the 80 samples yielding giant grains, abundance varies from 3 to > 250, with no systematic relationship to depositional facies. When normalized by volume of limestone processed (Table 1), the 3.5 m representing the upper Asselian section yielded ~ 2–3 times the concentration (116 kg^{-1}) of giant grains relative to the upper Kasimovian–lower Gzhelian (34 kg^{-1}) and Moscovian (45 kg^{-1}) intervals, and a similar concentration of giant grains to the Artinskian (96 kg^{-1}). Due to the low sample volume and the potential for grains to concentrate at a disconformity surface leading to potential skewing of data, Asselian data are included here for completeness, but are considered lower confidence owing to the disconformity-truncated section limited to ~3 m sampled.

Grain shape and composition vary as well (Figure 3). Grain shapes range from well-rounded to very angular, with rounded grains commonly exhibiting surface pitting. Rounded grains are most commonly quartz, or subordinately orthoclase and plagioclase. Subangular-angular grains common in all study intervals include quartz, orthoclase, plagioclase, and igneous rock fragments. Rock fragments exhibit varying compositions (quartz+sanidine, quartz+orthoclase+albite, orthoclase+plagioclase+hornblende,

etc.) ranging from intermediate to felsic. A special class of angular grains occurs, characterized by a vesicular texture, very high silica contents (up to 80%), and conchoidal fracturing. The vesicles, bubble walls, conchoidally fractured surfaces, and lack of visible minerals mark these as particles of volcanic glass, likely of rhyolitic composition based on the high silica content, close alignment of Al to summed Na+K+Ca, and minor but significant FeO (~.5-1.5%). Sanidine and local accessory phases (e.g., zircon) occur uniquely in the Artinskian section. Of the nine lithic fragments that exceed the sand-size fraction, all contain a predominantly albitic matrix, with amphibole, and quartz, with lesser amounts of minerals comprising titanite, potassium feldspar, ilmenite, biotite, hematite, and chlorite. These compositions are most closely affiliated with intermediate — felsic volcanism, however due to the size of these grains, flow textures inhibiting observation of grain boundaries, and the similarity between albite and quartz in backscattered electron imaging, these lithics cannot be named with absolute confidence. They appear, based on the data available, to be of andesitic — rhyolitic composition.

Pseudomorphs of giant grains that consist of clay minerals with small inclusions of quartz, albite, potassium feldspar, mica, and Cr and Ti oxides also occur. The clay matrix chemistry is dominated by silica with lesser quantities of Al, Fe, K, and Na. This matrix chemistry matches or is very similar to the compositions of the volcanic glass particles that occur throughout the studied sections, suggesting these are fragments of altered glass (Appendix 2).

Results—Grain Origins

The shapes and compositions of the giant grains indicate two origins: 1 – eolian transport from continental sources for the rounded grains (mostly quartz, subordinate feldspar), and 2 – eolian fallout from volcanic sources for the angular grains of igneous composition. The rounded shapes and commonly pitted surface textures of the rounded grains are consistent with a prior history of eolian saltation (Smith et al., 2018). In contrast, the occurrence of angular grains comprising high-silica volcanic glass, sanidine, orthoclase, quartz, (minimal) anorthite, and large lithic fragments of likely andesitic — rhyolitic composition indicate an igneous (volcanic) source that ranges from intermediate to felsic.

Of the random sampling of giant grains analyzed, the ratio of volcanic to continentally derived grains averages 27:1 (ignoring the 3:1 ratio displayed in the low confidence Asselian) with ratios of 55:1, 13:1, and 14:1 for the Moscovian, Kasimovian – Gzhelian, and Artinskian, respectively (Table 1).

Radiogenic isotopic data ($^{87}Sr/^{86}Sr$ and ϵ_{Nd}) were obtained on three large (cm-size) lithic clasts and several samples of co-associated fine (<180 μm) dust fractions to supplement the mineralogical data in assessing sources and possible provenance regions (Figure 4). Three Moscovian lithic fragments display $^{87}Sr/^{86}Sr$ values ranging from 0.705136 to 0.705260 and ϵ_{Nd} values ranging from + 0.9 to +1.1, values typical of many volcanic arc settings (White, 2015). When ϵ_{Nd} values are back calculated to their initial values at 300 Ma, ϵ_{Nd} values range from +3.8 to +4.0, consistent with island arc/juvenile continental arc sources (White, 2015). Six samples of the Moscovian/Gzhelian fine fraction exhibit more radiogenic $^{87}Sr/^{86}Sr$ values of 0.706405 to 0.726455, and less radiogenic ϵ_{Nd} values of -1.9 to -7.5, consistent with source regions containing components of older continental crust (Figure 4).

Results – Provenance

Continental Provenance

Continental grains (rounded quartz and feldspar) reflect deflation from arid/semi-arid regions capable of dust emission, and presumably within relatively low latitudes, given the equatorial setting of the Akiyoshi atoll. Candidate dust-emission regions should exhibit proxy evidence for arid- or semi-arid conditions (e.g., widespread evaporite, and/or arid-semiarid paleosols), and negative evidence for perhumid conditions (Figure 1) (e.g., coal). To assess this, we rely on the stage-level global compilations of Boucot et al. (2013) and additional sources.

The nearest continental regions capable of potentially sourcing the dust are the North China and Tarim (NC&T) and South China (SC) blocks ~1,500 km (SC; Pangaea A)- ~4,500 km (NC&T; Pangaea A) and ~6,500km (SC; Pangaea B)–~8,500km (NC; Pangaea B) distant, and west of the Akiyoshi atoll. The South China block hosted peat (coal) and marine carbonate deposition from Moscovian through

Asselian times (e.g., Peng et al., 1999; Boucot et al. 2013), precluding this area as a viable dust emission region until the Artinskian. While North China and Tarim also exhibit coal deposition throughout the late Paleozoic (Boucot et al., 2013), evidence of fluctuating arid — humid or semi-arid – humid climate at and above ~15°N (Pangaea B)- ~30°N (Pangaea A) occurs in the form of evaporites intercalated with mudstone, sandstone and conglomerate in inferred floodplain strata of the Ahne coalfield, Central North China, and the Fengchen Formation, Junggar Basin (Boucot et al., 2013; Wang et al., 2020; Li et al., 2021). Nodular gypsum in discrete horizons of the Ahne coalfield suggests intermittent aridity in North China during the Late Carboniferous – Early Permian; however, a deltaic – alluvial plain setting is not conducive to production of widespread grain pitting typical of eolian saltation (Li et al., 2021). Given the paleolatitude of North China and Tarim (20 — 45°N), this source would require transport from the extratropical region, and westerly/northwesterly (monsoonal) atmospheric circulation over the Paleo-Tethys. The latter scenario is a persistent feature in the simulations of Heavens et al. (2012, 2015) and appeared to be decoupled from the better-known Pangaean megamonsoon (Kutzbach and Gallimore, 1989; Heavens et al., 2012; Kiehl and Shields, 2018). Alternatively, possible continental source regions also lie farther west of the Akiyoshi Terrane, in eastern equatorial Pangaea (Eastern Europe and North-Central Africa); however, excepting parts of North Africa, these regions were perhumid through the Pennsylvanian, becoming more arid in the Permian (Schneider et al., 2006; Tabor et al., 2008; Boucot et al. 2013; Michel et al., 2015). Additionally, emission from eastern equatorial Pangaea would require >10,000 km of westerly transport for Pangaea A and >14,000 km of westerly transport for Pangaea B. Middle Pennsylvanian–Lower Permian strata of western equatorial Pangaea record widespread evidence for the requisite aridity, including eolian strata (Kessler et al. 2001; Boucot et al. 2013), and this region lies upwind of the Akiyoshi Terrane if zonal circulation prevailed, but implies ~10,000 km (Pangaea B)-~20,000 km (Pangaea A) of atmospheric transport.

Volcanic Provenance

Volcanic components reflect derivation from sites of intermediate to felsic volcanism situated at latitudes < 45°, to enable transport to equatorial regions such as the Akiyoshi Terrane. Potential modern analog arc systems with comparable compositions include the Taupo Volcanic Zone (New Zealand) which displays a close affinity to a back-arc basin transitioning from oceanic to continental crust (McCulloch et al., 1994), the Japanese island arc system (Hokkaido, Japan; Takanashi et al., 2012), and the Sierra La Primavera continental margin arc system in Mexico (Mahood and Halliday, 1988).

Proximity to the Akiyoshi Terrane, volcanic compositions, and Nd and Sr isotope data were assessed against published data on active volcanism during the study intervals (compiled in Soreghan et al., 2019) to determine the most likely volcanic source(s), resulting in two options: eastern equatorial Pangaea, and North China (Figure 1). While the most proximal volcanism was that accompanying the obduction of the Akiyoshi Terrane onto proto-Japan in the late Permian, Akiyoshi-associated volcanism dates to the early Permian, so cannot account for the evidence for volcanism observed in the upper Carboniferous part of the section—including the giant lithic fragments (Minato et al., 1962). In contrast, the volcanism in the Tianshan, Junggar, Tarim, and Mongolian regions of the North China block and the Central Asian Orogenic Belt during the Moscovian – Artinskian study interval spans mafic – intermediate – felsic compositions (Su et al., 2012; Lai et al., 2014; Wie et al. 2017; Chen et al., 2020). Felsic material of Moscovian age from the Chinese regions displays $^{87}Sr/^{86}Sr$ isotope values of 0.702272 – 0.705580, and initial ϵNd values of 2.8 – 7.4 (Su et al., 2012; Tong et al., 2018), overlapping values from the large lithic fragments recovered from the Moscovian section ($^{87}Sr/^{86}Sr$ of 0.705136-0.705260 and ϵNd_i of 3.8 – 4.0). Abundant records of felsic (dacitic to rhyolitic) volcanism spanning all study intervals occur in eastern equatorial Pangaea (western-central Europe; e.g., Breitkreuz and Kennedy, 1999; Capuzzo and Busy, 2000; Koniger et al., 2002; Breitkreuz et al., 2007; Awdankiewicz et al., 2013). Available $^{87}Sr/^{86}Sr$ values for such volcanism ranges from 0.7100 - 0.7128, compared to the Akiyoshi giant lithic fragments with values of ~0.705 (Romer et al., 2001; Koniger and Lorenz 2002), and ϵNd values ranging from -6.7 to -7.0, falling far outside the range of ϵNd_i values (+3.8 to +4.0) of the Akiyoshi giant lithic fragments

(Romer et al., 2001). However, these values do overlap with those of the fine fraction from the Akiyoshi dust, meaning eastern equatorial Pangaean volcanism cannot be excluded as a potential source for the Akiyoshi fine fraction. The most parsimonious interpretation, accounting for both compositional and age data suggests that the volcanism between the northern margin of the North China Block and the southern margin of Tarim, and within the Central Asian Orogenic Belt likely sourced the giant lithic fragments to the Akiyoshi Terrane but could not have been the sole source of all volcanic material. The wide range of both $^{87}Sr/^{86}Sr$ and ϵNd suggests a mixing of multiple distal sources, and furthermore implies the operation of both northwesterly (China block) and westerly (eastern equatorial Pangaea) circulation.

Prevailing atmospheric wind directions and velocities play large roles in controlling tephra fallout (Fischer and Schminke, 1984; Woods et al., 1995; Jenkins et al., 2016). Thus, the likely sourcing of volcanic dust that included both large lithic fragments as well as fine dust to the Akiyoshi Terrane during the Moscovian implies a significant component of westerly circulation, reinforcing the presence of monsoonal circulation over the Paleo-Tethyan region. Western equatorial Pangaea is eliminated as a potential continental source because it would require prevailing zonal easterlies while the most likely source for the (distinctive) giant lithic fragments requires westerlies, and it requires a significantly longer transport distance.

Discussion

Data from the Akiyoshi Limestone establish that the long-range transport of giant grains is not limited to modern/Holocene or – in one case of giant grains recovered from a Greenland ice core—Pleistocene conditions. Most of the giant grains documented in the previous literature all come from the Holocene — Pleistocene representing continental dust sourced from the Sahara and Asia; however, two studies documented giant grains of volcanic origin (Betzer et al., 1988; Hayasaka et al., 1990; Ram and Gayley, 1991; Van Maldern et al., 1992; Arimoto et al., 1997; Middleton et al., 2001; Van der Does et al. 2018). These studies (Ram and Gayley, 1991; Lundberg and Mcfarlane, 2012) documented grains (up to 300 μm

and 190 μm, respectively) at least 1,000 km from their sources, and noted the implication of significant stratospheric injection, thus requiring a high (~7) volcanic explosivity index (VEI; Fischer and Schminke, 1984). In light of these studies, the occurrence in the Akiyoshi Limestone of lithics of up to 2 cm that traveled ~4,500 km (Pangaea A)- ~8,500 km (Pangaea B), requires stratospheric injection, likely together with other mechanisms to extend atmospheric transport distance. Van der Does et al. (2018) noted four potential mechanisms capable of enhancing atmospheric transport of giant grains: 1) High atmospheric windspeeds reducing the time it takes for a particle to travel a given distance; 2) turbulence resulting in repeated relofting of particles thus extending residence time in the atmosphere; 3) triboelectrification in which collision of like-charged particles forms a "charged cloud" capable of increasing buoyancy of particles; 4) tropical cyclone events, in which particles can be ejected from the top of the storm system to higher atmospheric altitudes.

Mineralogic, grain shape, and isotopic evidence indicate influx of both continental and volcanic sourcing of grains to the Akiyoshi atoll. Continental grains of up to 200 μm (long-axis) were transported from North China (~4500 km - ~8,500 km distant) and/or eastern equatorial Pangaea (~10,000 km - ~14,000 km distant), both requiring westerly circulation at low latitudes. Large lithics transported from between the northern margin of North China and southern margin of Tarim (>4,500 km) range in size from 0.5-2.5 cm, while the remaining volcanic grains of up to 1 mm (long-axis) were likely transported from multiple sources including eastern equatorial Pangaea and the North China—Tarim region —again, both requiring westerly atmospheric circulation. Westerly flow at the equatorial latitude of the Akiyoshi atoll implies the presence of a monsoonal circulation pattern (Riehl, 1954). Accepting Heavens et al.'s (2012) model results of persistent monsoonal circulation over Paleo-Tethys decoupled from that over Pangaea, summer westerlies would have been a sustained feature over the Akiyoshi atoll during late Paleozoic time.

Assuming minimal variability in the strength or seasonal duration of westerly flow over the Akiyoshi atoll, significant variability in both the concentration and origin (volcanic versus continental) of the grains through time (Table 1) reveals information on trends in explosive volcanism and continental aridity of

source regions. The exclusive presence of giant (up to 2 cm) lithic fragments in the Moscovian interval suggests that, while more giant grains accumulated in the Akiyoshi Limestone during the Early Permian, highly explosive volcanism was more common in the Middle Pennsylvanian. The apparent twofold increase in volcanically sourced grain concentrations in the Permian relative to the Pennsylvanian thus may indicate more efficient transport of volcanic giant grains. This increase in transport efficiency is most likely a result of the proto-Japanese arcs and the Ailaoshan volcanic belt volcanism, which transitioned to more felsic (and generally more explosive) compositions in the Early Permian, corresponding to the predominantly felsic composition of grains extracted from the Akiyoshi Limestone (Minato et al., 1962; Lai et al., 2013). These regions are not viable sources for continental grains, indicating that while potential sources of volcanic grains were closer to the Akiyoshi atoll during the Permian than the Late Carboniferous, potential sources of aridity remained farther removed. Even compensating for this effect, the threefold to tenfold apparent increase in continentally sourced grains in the Permian implies a 50–400% increase in giant grain emission at source, suggesting that viable dust-bearing continental sources expanded through time, consistent with widespread continental aridification in low latitudes through the Permian (Boucot et al., 2013).

The Akiyoshi Limestone served as a remarkable dust trap within the vast Panthalassic Ocean, capturing snapshots of both instantaneous events (eruptions) and climatic evolution of distant regions. In addition to more typical fine-grained dust in deep time, giant-grain records such as this represent a powerful tool for exploring extremes of volcanism and eolian transport in deep time.

Figure Captions

Figure 1: A) Pangaea A reconstruction and B) Pangaea B reconstruction for 300 Ma (Pangaea A; Domeier and Torsvik, 2014) and 290 Ma (Pangaea B; Kent and Muttoni, 2020). The blue ellipse highlights the location of the Akiyoshi atoll and its projected migration;red triangles denote possible volcanic sources, and the orange ellipses highlight regions capable of sourcing continental dust to the Akiyoshi atoll. C) displays the modern location of the Akiyoshi Terrane in southwestern Japan.

Figure 2: Stratigraphic column indicating the sampled sections of the Akiyoshi Limestone. The light blue column with scattered brick pattern indicates the Akiyoshi Limestone as a predominantly massive carbonate unit. The four columns marked A, B, C, and D highlight the horizons containing giant grains (denoted by small dots) and giant lithic fragments (denoted by large squares). Horizontal curved line in column C denote the disconformity with uppermost Asselian strata beneath the unconformity and upper Artinskian strata above. Straight horizontal lines near the top of each section with "TS" displayed above indicate the top of section.

Figure 3: Photomicrographs (SEM) and photographs of the giant grain types within the Akiyoshi Limestone.

Figure 4: ϵ_{Nd} vs $^{87}Sr/^{86}Sr$ graph with typical value envelopes for the mantle array denoted by gray oval. The upper left field in this graph is most commonly attributed to mid-ocean ridge basalts (MORBs), while the Nd-Sr mantle array defined by oceanic and continental volcanic rocks trends downward towards differentiated upper continental crust (White, 2015). Red squares represent the individual giant lithic fragments in the Akiyoshi Limestone, while the black star displays the average back calculated initial isotopic values for the giant lithics. The giant lithic grains plot towards more juvenile island and/or continental arc signatures, meaning their calculated initial ratios for 300 Ma are consistent with many island and continental arc settings with felsic magmatism (examples plotted). In contrast, the Akiyoshi fine-grained material, depicted by blue diamonds, contains a higher percentage of older, more evolved crustal components consistent with upper continental crust sources. 2 Akiyoshi fine samples plot directly beneath the Akiyoshi Giant Lithic, and thus are not visible on the graph. Colored rectangles superimposed

on this figure depict selected modern felsic analog arcs within the circum-Pacific belt with similar Sr and/or Nd isotopic values to the large lithic fragments found in the Akiyoshi Limestone.

Figures

Figure 1

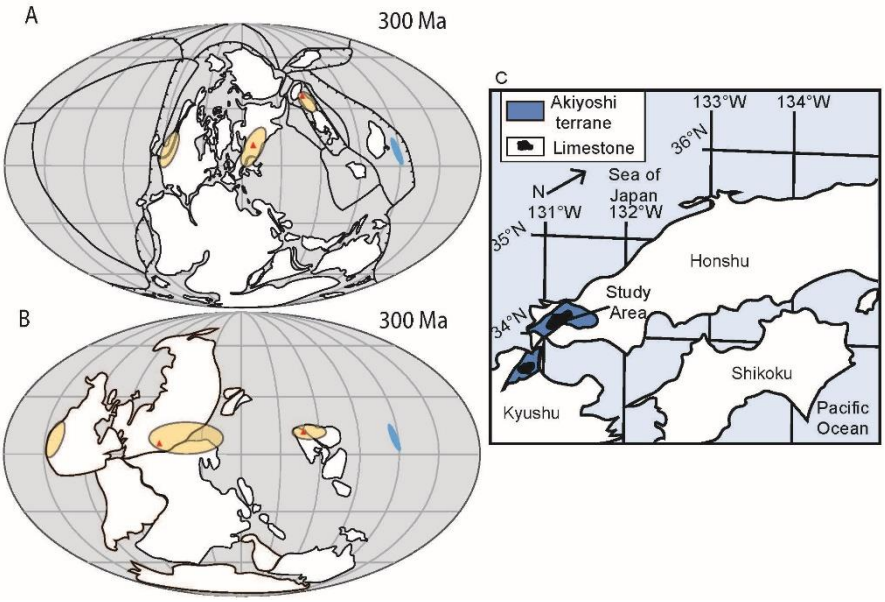

Figure 2

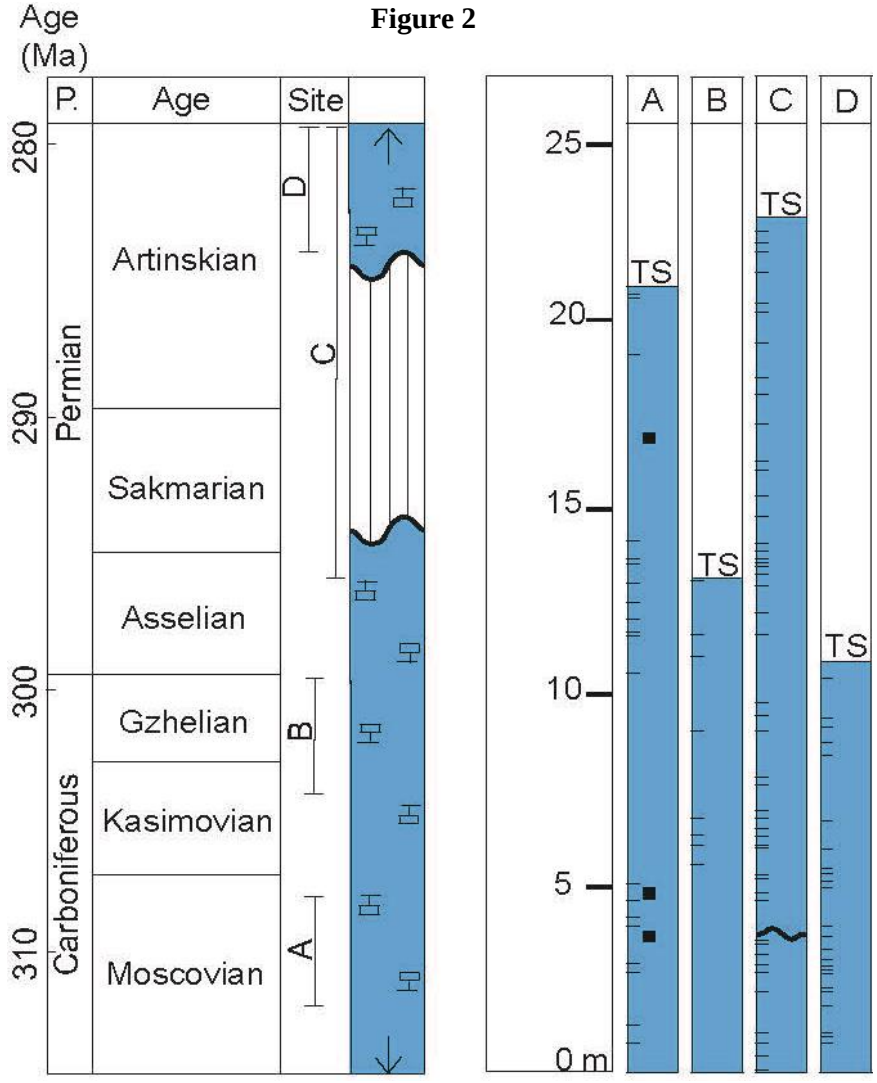

Figure 3

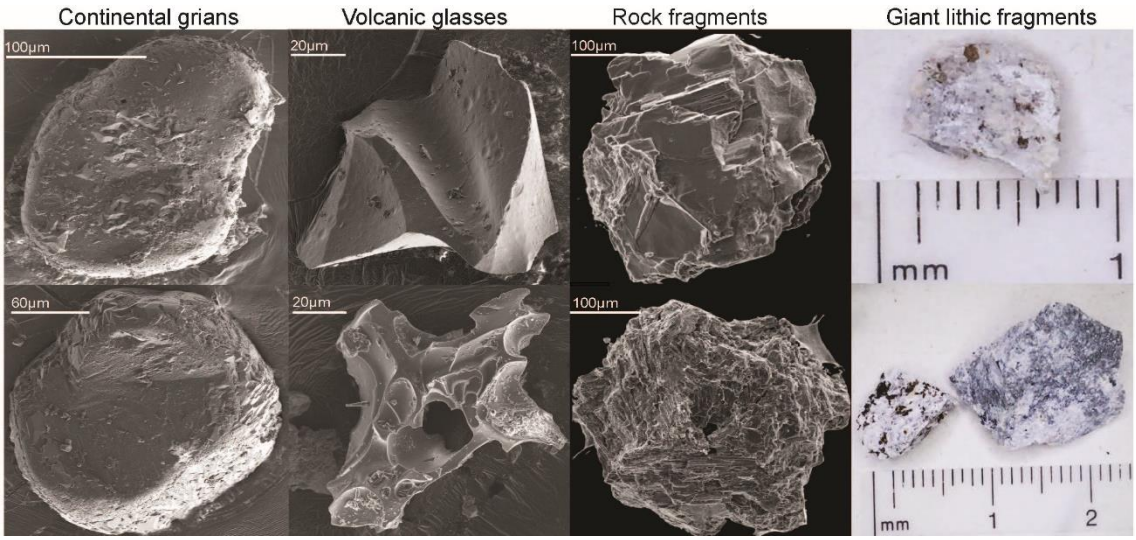

Figure 4

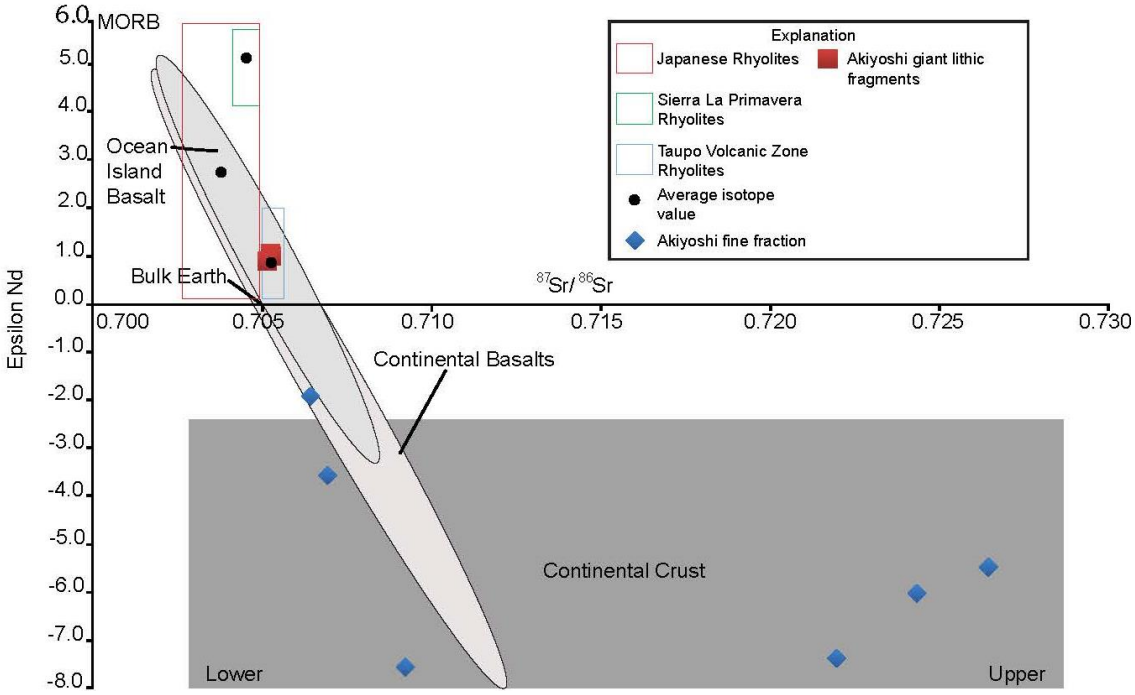

Tables

Table 1. Dust Data

Age	# of horizons sampled	# of grains	# of grains analyzed	Avg. starting mass of LS	Grains/kg of LS	Largest grain long axis (µm)	Avg. long axis (µm)	Vol.:Con.
Art.	100	2,626	966	272	96	633	221	14:1
Ass.	21	606	121	300	116	650	262	3:1
Gzh.	49	176	91	107	34	1215	475	17:1
Mos.	113	1150	135	228	45	2000	202	67:1

Table depicting dust data for each time period in which dust deposition is recorded. Data included from left to right is the number of horizons sampled, number of detrital grains extracted, number of detrital grains subsequently analyzed, average starting mass of limestone, number of grains per kg of limestone, largest grains long axis in microns, average grain size in microns, and the ratio of volcanic to continental grains. The average aspect ratio of Akiyoshi giant grains is 2:3. It is worth noting that the number of volcanic grains per kg of limestone is 44/kg, 32/kg, 87/kg, and 89/kg for each time period analyzed from Moscovian —Artinskian, and that the number of continental grains per kg of limestone is 1/kg, 2/kg, 29/kg, and 7/kg for each time period analyzed from Moscovian — Artinskain.

References

Adebiyi, A. A., Kok, J. F. (2019). Climate models miss most of the coarse dust in the atmosphere. Science Advances V. 6, No. 15

Arimoto R., Ray B.J., Lewis N.F., Tomza U., and Duce R.A. (1997). Mass-particle size distribution of atmospheric dust and the dry deposition of dust to the remote ocean. Journal of Geophysical Research, V. 102, i. D13, p. 15867-15874

Awdankiewicz, M., Kryza, R., and Szczepara, N. (2013) Timing of post-collisional volcanism in the eastern part of the Variscan Belt: constraints from SHRIMP zircon dating of Permian rhyolites in the North-Sudetic Basin (SW Poland). Geological Magazine. 151(04): p. 611-628.

Becq-Giraudon J.F., Montenat C., Van Den Driessche J. (1996). Hercynian high-altitude phenomena in the Frencg Massif Central: tectonic implications. Paleogeography, Paleoclimatology, Paleoecology. V. 122, p.227-241.

Beget J. E., Keskinen M., Severin K. (1993). Mineral particles from Asia found in volcanic loess on the island of Hawaii. Elsevier Science Publishers. Sedimentary Geology V. 84. P. 189-197.

Betzer P. R., Carder K. L., Duce R. A., Merrill J. T., Tindale N. W., Uematsu M., Costello D. K., Young R. W., Feely R. A., Breland J. A., Bernstein R. E., Greco A. M. (1988). Long-range transport of giant mineral aerosol particles. Nature. V. 336. P. 568-71.

Bishop J.W., Montañez I.P., Osleger D.A. (2010). Dynamic Carboniferous climate change, Arrow Canyon, Nevada. Geosphere. V.6 i.1 p. 1-34.

Boucot A. J., Xu C., Scotese C. R., Morley J. R. (2013). Phanerozoic Paleoclimate: An Atlas of Lithologic Indicators of Climate.

Boyd, P., Watson, A., Law, C. et al. (2000). A mesoscale phytoplankton bloom in the polar Southern Ocean stimulated by iron fertilization. *Nature* v. 407, p. 695–702.

Breitkreuz, C. and A. Kennedy (1999). Magmatic flare-up at the Carboniferous=Permian boundary in the NE German Basin revealed by SHRIMP zircon ages. Tectonophysics 302: p. 307-326.

Breitkreuz, C., Kennedy, A., Geissler, M., Ehling, B.C., Kopp, J., Muszynski, A., Protas, A., Stouge, S. (2007). Far Eastern Avalonia: Its chronostratigraphic structure revealed by SHRIMP zircon ages form Upper Carboniferous to Lower Permian volcanic rocks (drill cores from Germany, Poland, Denmark). GSA Special Papers V. 423.

Capuzzo, N. and F. Busy (2000). High-precision dating and origin of synsedimentary volcanism in the Late Carboniferous Salvan-Dorenaz basin (Aiguilles-Rouges Massif, Western Alps). Schweiz Mineral Petrogr Mitt 80: p. 147-167.

Chen, G., Liu, R., Deng, T., Wang, L. (2020). Bimodal Magmatism produced by delamination: geochemical evidence from late Paleozoic volcanic rocks form the Yili Block, Western Tianshan, Northwestern China. Geological Magazine

Domeier M. and Torsvik T.H. (2014). Plate Tectonics in the late Paleozoic. Geoscience Frontiers V. 5 p. 303-350.

Fielding C.R., Frank T.D., Birgenheier L.P., Rygel M.C., Jones A.T., (2008). Stratigraphic imprint of the Late Paleozoic Ice Age in eastern Australia: a record of alternating glacial and nonglacial climate regime. Geol. Soc. London J. v.165, p. 129-140.

Heavens N.G., Mahowald N.M., Soreghan G.S., Soreghan M.J., Shields C.A. (2015). Paleogeography, Paleoclimatology, Paleoecology. V. 425, p. 109-127.

Heavens, N.G., N.M. Mahowald, G.S. Soreghan, M.J. Soreghan, C.A. Shields, 2012, Glacial-Interglacial Variability in Tropical Pangaean Precipitation during the Late Paleozoic Ice Age: Simulations with the Community Climate System Model, *Climate of the Past Discussions*, 8**,** 19151972;

Heckel P. (1993) Evaluation of evidence for Glacial-Eustatic Control over Marine Pennsylvanian Cyclothems in North America and Consideration of Possible Tectonic Effects. SEPM Special Publications.

Isbell J.L., Miller M.F., Wolfe K.L., and Lanaker P.A. (2003). Timing of late Paleozoic glciations in Gondwana: was glaciation responsible for the development of Northern Hemisphere Cyclothems?

In: M.A. Chan and A.W. Archer (Editors). Extreme Depositional Environments: Mega End Members in Geologic Time. Geol. Soc. Am. Spec. Pap. V. 370, p. 5-24.

Jenkins, S.F., Wilson, T., Magill C., Miller, V., Stewart, C., Blong, R., Marzocchi, W., Boulton, M., Bonadonna, C., Costa, A. (2015). Volcanic ash fall hazard and risk. Cambridge University Press. P. 173-222.

Kanmera K. and Nishi H. (1983). Accreted oceanic reef complex in southwest Japan. In: M. Hashimoto and S. Uyeda (Editors). Accretion Tectonics in the Circum-Pacific Regions, Terra Publications, Tokyo. p. 195-206.

Kanmera K., Sano, H., and Isozaki, Y. (1990). Akiyoshi Terrane. In: k. Ichikawa, S. Mizutani, I. Hara, S. Hada, and A. Yao (Editors). Pre-Cretaceous terranes of Japan. Int. Geol. Correl. Project, V. 244, p. 49-62.

Karydis, V. A., Kumar, P., Barahona, D., Sokolik, I. N., and Nenes, A. (2011), On the effect of dust particles on global cloud condensation nuclei and cloud droplet number, *J. Geophys. Res.*, 116, D23204

Kasuya, A., Isozaki, Y., Igo, I., 2012. Constraining paleo-latitude of a biogeographic boundary in mid-Panthalassa: Fusuline province shift on the Late Guadalupian (Permian) migrating seamount. Gondwana Res. 21, 611–623.

Kent, D.V. and Muttoni, G. (2018). Pangaea B and the Late Paleozoic Ice Age. Paleogeography, Paleoclimatology, Pleoecology.

Kessler, J. L. P., Soreghan, G. S., Wacker, H. J.; Equatorial Aridity in Western Pangea: Lower Permian Loessite and Dolomitic Paleosols in Northeastern New Mexico, U.S.A.. *Journal of Sedimentary Research* 2001;; 71 (5): 817–832.

Kirschvink, J. L., Isozaki, Y., Shibuya, H., Otofuji, Y., Raub, T. D., Hilburn, I. A., Kasuya, T., Yokoyama, M., Bonifacie, M. (2015). Challenging the sensitivity limits of Paleomagnetism: Magnetostratigraphy of weakly magnetized Guadalupian–Lopingian (Permian) Limestone from Kyushu, Japan. Palaeogeography, Palaeoclimatology, Palaeoecology. V. 418, p. 75-89.

Kok, J. F., Ridley, D. A., Zhou, Q., Miller, R.L., Zhao, C., Heald, C. L., Ward, D. S., Albani, S., Haustein, K. (2017). Smaller desert dust cooling effect estimated from analysis of dust size and abundance. Nat. Geosci. V. 10 p . 274-278.

Koniger, S., Lorenz, V., Stollhofen, H., Armstrong, R. (2002) Origin, age and stratigraphic significance of distal fallout ash tuffs from the Carboniferous-Permian continental Saar-Nahe Basin (SW Germany). International Journal of Earth Sciences 91(2): p. 341-356.

Kutzbach, J. E., and Gallimore, R. G. (1989), Pangaean climates: Megamonsoons of the megacontinent, *J. Geophys. Res.*, 94(D3), 3341– 3357, doi:10.1029/JD094iD03p03341

Lai, K., Meffre, S., Crawford, A.J., Zaw, K., Xue, C., Halpin, J.A. (2014). The Western Ailaoshan Volcanic Belts and their SE Asia connection: A new tectonic model for the Eastern Indochina Block. Gondwana Research 26(1): p. 52-74.

Li, Y., Shao, L., Fielding, C.R., Wang, D., and Mu, G. (2021), Sequence stratigraphy, paleogeography, and coal accumulation in a lowland alluvial plain, coastal plain, and shallow-marine setting: Upper Carboniferous-Permian of the Anyang-Hebi coalfield, Henan Province, North China, Paleogeography, Paleoclimatology, Paleoecology, V. 567

Lundberg, J., McFarlane, D.A. A significant middle Pleistocene tephra deposit preserved in the caves of Mulu, Borneo, Quaternary Research (2012), doi 10.1016/j.yqres.2012.01.007.

Mahood, G.A. and Halliday, A.N. (1988) Generation of high silica rhyolite: A Nd, Sr, and O isotopic study of Sierra La Primavera, Mexican Neovolcanic Belt. Contrib Mineral Petrol V. 100 p. 183-191).

Mahowald, N.M. (2011). Aerosol indirect effect on biogeochemical cycles and climate. Science, V. 334, p.794–796

Mahowald N.M., Kiehl L.M. (2003). Mineral aerosol and cloud interactions. Geophysical Research Letters. V.30 I. 9

McCulloch, M.T., Kyser, T.K., Woodhead, J.D., Kinsley, L. (1994). Pb-Sr-Nd-O isotopic constraints on the origin of rhyolites from the Taupo Volcanic Zone of New Zealand: Evidence for assimilation followed by fractionation from basalt. Contrib Mineral Petrol V.115 p. 303-312.

Michel, L. A., Tabor, N. J., Montanez, I. P., Schmitz, M. D., & Davydov, V. I. (2015). Chronostratigraphy and paleoclimatology of the lodeve basin, 22urope; evidence for a pan-tropical aridification event across the Carboniferous-Permian boundary. *Palaeogeography, Palaeoclimatology, Palaeoecology*, *430*, 118-131.

Middleton N.J., Betzer P.R., Bull P.A. (2001). Long-range transport of 'giant' aeolian grains: linkage with discrete sedimentary sources and implications for protective particle transfer. Marine Geology V. 177, p. 411-417.

Minato, M., Takeda, H., Kato, M., (1962). ON THE VOLCANIC ROCKS IN THE JAPENESE LATE PALEOZOIC, SECOND REPORT – CARBONIFEROUS. International Geology Review, 4:5, 590-594.

Montañez I. P., Poulsen C. J. (2013). The Late Paleozoic Ice Age: An Evolving Paradigm. Annu. Rev. Earth Planet. Sci. V. 41, p. 629-56.

Moringa, H., Inokuchi, H., Domen, H., Yaskawa, K., Kawano, M. (1988). Paleomagnetism of the Akiyoshi Limestone: Evidence for Secondary Magnetization. Journal of geomagnetism and geoelectricity. V. 41, p. 89-99.

Muller, R. D., Sdrolias, M., Giana, C., Roest, W.R. (2008). Age, spreading rates, and spreading asymmetry of world's ocean crust. Geochemistry Geophysics Geosystems. V. 9, N. 4.

Nakazawa, T. and Ueno, K. (2004). Sequence boundary and related sedimentary and diagenetic facies formed on Middle Permian mid-oceanic carbonate platform: Core observation of the Akiyoshi Limestone, Southwest Japan. Facies. V. 50, p. 301-311

Nenes, A., Murray, B., Bougiatioti, A. (2014). Mineral Dust. Springer Netherlands, Dordrecht. P 287-325

Patterson E. M. (2011). Fluctuation dust in the Late Paleozoic ice house: records from an oceanic atoll, Akiyoshi, Japan. University of Oklahoma Masters Thesis.

Peng, G., Zhong, R., & Tang, W. (1999). The relationship between the coal accumulating process and upper carboniferous-early lower 23uropea transgression-regression on the western margin of the north china platform. Gudili Xuebao = Journal of Palaeogeography, 1(2), 18-27.

Pfeifer, L.S., Soreghan, G.S., Pochat, S., Van Den Driessche, J. (2020). Loess in eastern equatorial Pangea archives a dusty atmosphere and possible upland glaciation. GSA Bulletin, in press.

Pyle, D.M. (1989). The thickness, volume, and grainsize of tephra fall deposits. Bulletin of Volcanology. V. 51 p. 1-15.

Qi, X. (2016). An icehouse dust record from the upper Paleozoic (Asselian-Artinskian, Moscovian) Akiyoshi limestone (Japan). University of Oklahoma Masters Thesis.

Ram, M. and Gayley, R. I. (1991). Long-range transport of volcanic ash to the Greenland ice sheet. Nature. V. 349. P. 401-404.

Riehl, H. (1954) Tropical Meteorology. McGraw-Hill, New York, pp. 3–4.

Romer, R.L., Forster, H.J., Breitkreuz, C. (2001) Intracontinental extensional magmatism with a subduction fingerprint: the late Carboniferous Halle Volcanic Complex (Germany). Contrib Mineral Petrol V. 141 p 201-221.

Sano H., Kanmera K. (1998). Paleogeographic reconstruction of accreted oceanic rocks Akiyoshi, southwest Japan. Geology, V. 16, p. 600-603.

Sano H., Kanmera K. (1991). Collapse of ancient oceanic complex- what happened during the collision of of Akiyoshi reef complex? Geologic setting and age of Akiyoshi terrane rocks on the western Akiyoshi-dai plateau. J. Geol. Soc. Japan. V. 97, p. 113-133.

Schneider, J. W., Koerner, F., Roscher, M., Kroner, U., & Buggisch, W. (2006). Permian climate development in the northern peri-tethys area; the lodeve basin, 23urope massif central, compared in a 23uropean and global context. *Palaeogeography, Palaeoclimatology, Palaeoecology, 240*(1-2), 161-183.

Shields, C.A. and J.T. Kiehl, Monsoonal precipitation in the Paleo-Tethys warm pool during the latest Permian, *Palaeogeography, Palaeoclimatology, Palaeoecology*, 491, 123–136**,** doi: 10.1016/j.palaeo.2017.12.001

Smith, C., Soreghan, G.S., Ohta, T. (2018). Scanning electron microscope (SEM) microtextural analysis as a paleoclimate tool for fluvial deposits: A modern Test. GSA Bulletin.

Soreghan G.S., Soreghan M.J., Hamilton M.A. (2008). Origin and significance of loess in late Paleozoic Western Pangaea: a record of tropical cold?. Paleogeography, Paleoclimatology, Paleoecology. V. 268 p. 234-259.

Soreghan, G.S., Soreghan, M.J., Heavens, N.G. (2019). Explosive volcanism as a key driver of the late Paleozoic ice age. Geology V.47(7) p. 600-604

Su, Y., Zheng, J., Griffin, W.L., Zhao, J., Tang, H., Ma, Q., Lin, X. (2012). Geochemistry and geochronology of Carboniferous volcanic rocks in the eastern Junggar terrane, NW China: Implication for a tectonic transition. Gondwana Research V. 22 p. 1009-1029.

Sur, S., Soreghan M.J, Soreghan, G.S., Stagner, A.F. (2010). Extracting the silicate mineral fraction from ancient carbonate: Assessing the geologic record of dust. J. Sed. Res. V. 80, p. 1-7.

Tabor N. J., Poulsen C. J. (2008). Paleoclimate across the Late Pennsylvanian-Early Permian tropical paleolatitudes: A review of climate indicators, their distribution, and relation to paleophysiographic climate factors. Paleogeography, Paleoclimatology, Paleoecology. Vol. 268(3-4), p 293.

Takanashi, K., Kakihara, Y, Ishimoto, H., Shuto, K. (2012). Melting of Crustal rocks as a possible origin for Middle Miocene to Quaternary rhyolites of northeast Hokkaido, Japan: Constraints from Sr and Nd isotopes and major- and trace-element chemistry. Journal of Volcanology and Geothermal research. V 221-222 p. 52-70

Taira, Asahiko (2001) Tectonic Evolution of the Japanese Island Arc System. Annu Rev. Earth Planet. Sci. V. 29 p. 109-134.

Taylor, S.R. and McLennan, S.M. (1985) The Continental Crust: Its Composition and Evolution. Blackwell, Oxford, 312.

Tong, L., Li, Y., Li, G., Li, Z. Yang, G., Wang, Z., Wang, Z., Shen, R., Li, Z. (2018). Sr – Nd isotopes of Early and Late Carboniferous volcanic rocks in Yining Massif (Xinjiang, NW China): Implications for petrogenesis and tectonic evolution of Western Tianshan. Geological Journal V. 53 p 137-147.

Van Der Does M., Knippertz P., Zschenderlein P., Harrison R. G., Stuut J. W. (2017). The mysterious long-range transport of giant mineral dust particles. Science Advances V. 4 (12).

Van Malderen H., Rojas C., Van Grleken R. (1992). Characterization of Individual Giant Aerosol Particles above the North Sea. Environmental Science Technology. V. 26, p. 750-756.

Varga, G., Dagsson-Walhauserova, P., Gresina, F., Helgadottir, A. (2021). Saharan dust and giant quartz particle transport towards Iceland. Nature Scientific Reports 11:11891.

Wang, T., Cao, J., Carroll, A., Zhi, D., Tang, Y., Wang, X., Li, Y. (2020) Oldest preserved sodium carbonate evaporite: Late Paleozoic Fengcheng Formation, Junggar Basin, NW China. GSA Bulletin

White, W.M. (2015). Isotope Geochemistry: New Jersey, Wiley-Blackwell publishing, 318-362p.

Yu K., D'Odorico P., Bhattachan A., Okin G.S., Evan A.T. (2015) Dust-rainfall feedback in West African Sahel. Geophysics research letters. V. 42 p. 7563-7571.

Appendices

Appendix 1

Photos of the Akiyoshi Terrane study area. The first image shows the Akiyoshidai Quasi-National Park in the foreground with the Akiyoshi limestone sampling area in the forested region in the background. Image two is a photo within the woods of an exposure that was sampled for this work. The third photo is another example of the sampled limestone. Sections depicted in figure 2 are as follows: A = Uehata (34.27084°N, 131.33009°E), B = Managatake Mt. (34.26965°N, 131.32407°E), C = Guest House 3 (34.26673°N, 131.32410°E), and D = Guest House 2 (34.16001°N, 131.19419°E). Note in the third image the rare presence of a bedding plane within the Akiyoshi as well the overturned nature of the Akiyoshi Limestone.


0.8
1.0
1.1
1.2
1.3
1.4
1.5
1.6
1.7
GH

Appendix 2

Representative EDS spectra of glass and clay matrix from the Akiyoshi extracted grains. Note similarities in element peaks, compositions, and weight percents, indicating a potential link between the glass and subsequent clays. Variance in the appearance of tables and spectra graphs is due to the extended period of time (~10 years) between analyses displayed.

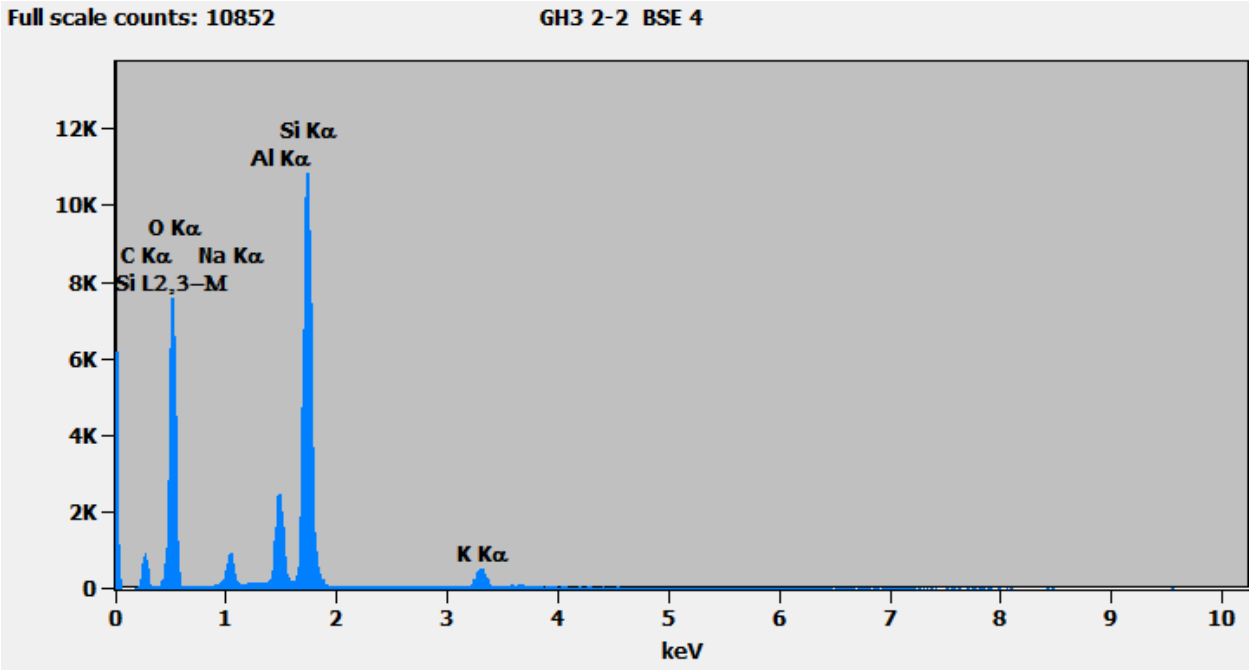

Live Time: 11.1 sec.

Acc.Voltage: 15.0 kV Take Off Angle: 47.1 deg.
Quantitative Results for: GH3 2-2 BSE 4

Element	*Weight %*	*Atom %*	*Formula*	*Compnd %*	*# Cations*
O	49.49S	63.33	(null)	---	---
Na	3.17	2.82	Na2O	4.27	0.356
Al	6.65	5.05	Al2O3	12.57	0.638
Si	36.53	26.63	SiO2	78.15	3.364
K	4.16	2.18	K2O	5.01	0.275
Total	100.00	100.00		100.00	4.633

Spectra of glass grain

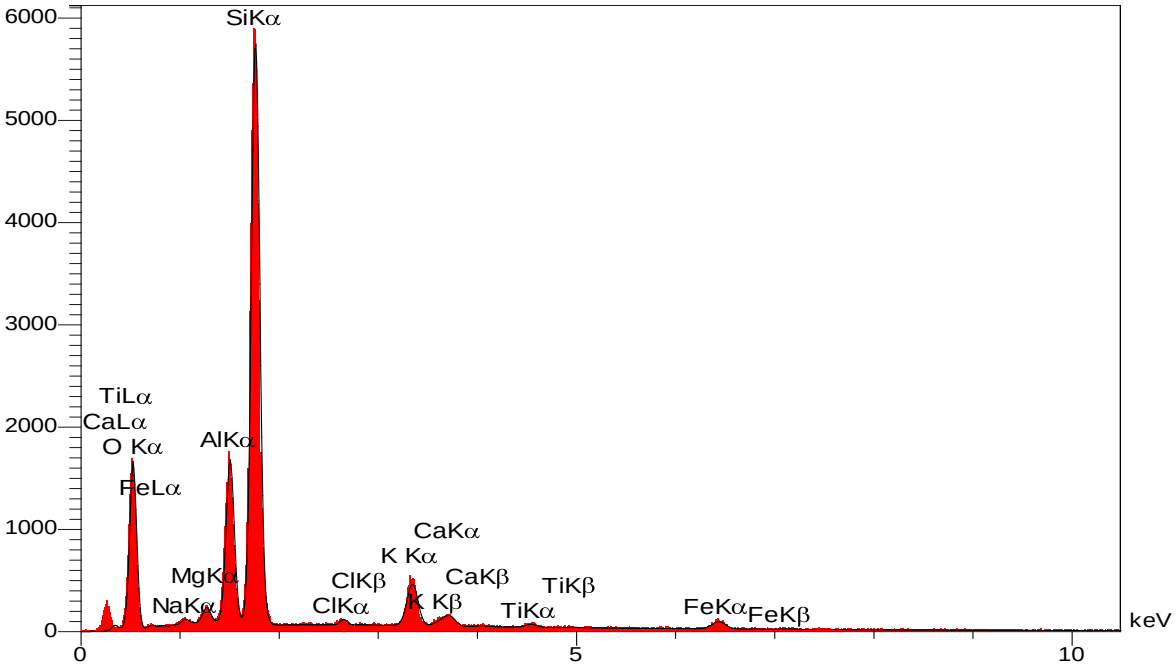

Measures & Results

Elt	Line	Int	W%	A%	Formula	Ox%	Cat#
O			48.88	63.52		0.00	0.00
Na	Kα	15.5	0.52	0.47	Na_2O	0.70	0.06
Mg	Kα	47.9	1.02	0.87	MgO	1.69	0.11
Al	Kα	541.5	9.20	7.09	Al_2O_3	17.39	0.89
Si	Kα	1958.5	33.05	24.47	SiO_2	70.71	3.08
Cl	Kα	14.8	0.30	0.18		0.30	0.02
K	Kα	188.0	3.94	2.10	K_2O	4.75	0.26
Ca	Kα	43.4	0.95	0.49	CaO	1.33	0.06
Ti	Kα	12.7	0.35	0.15	TiO_2	0.59	0.02
Fe	Kα	39.3	1.78	0.66	Fe_2O_3	2.55	0.08
			100.00	100.00		100.00	4.59

Spectra of clay matrix

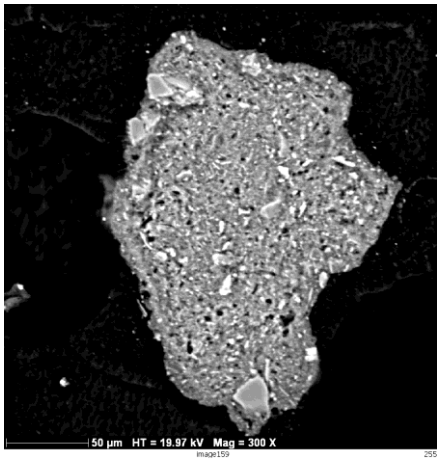

Appendix 3

Data for all giant grains extracted and analyzed from the Akiyoshi Limestone. The sites from which samples were collected are in the first column, the second column shows the stratigraphic height of the sample. Long axis and short axis measurements are in microns. Any notes taken at the time of analysis are also shown. Sample stubs with general stub notes have these notes located beneath all of the grain measurements. Samples were named based on site location abbreviations followed by height above base of section in meters. UHA 0.6 translates to Uehata 0.6 m above base of section. MNE 6.1 translates to Managatake Mt. 6.1 m above base of section. GH samples (GH2 and GH3) are named due to proximity to guest houses 2 and 3. The composition column gives mineralogical data about the grains where applicable, and the shape column provides information about grain shape, and when obvious, notes diagenetic properties of grains.

Site	Sampling Height (m)	Grain #	Long Axis	Short Axis	Comp.	Shape
UHA	0.6	1	265.00	70.00	qtz/clay?	subangular
		2	350.00	150.00	qtz/clay?	subangular
		3	50.00	50.00	glass	
		4	250.00	200.00	clay coat?	subrounded
		5	250.00	170.00	clay coat?	subangular
		6	600.00	350.00	clay coat?	very angular
		7	250.00	100.00	plg/kspr/qtz?	subangular
		8	200.00	100.00	clay coat?	subrounded
		9	150.00	100.00	clay coat?	subrounded
		10	150.00	150.00	clay coat?	subangular
		Average	**273.89**	**154.44**		
UHA	2.5	1	75.00	50.00	Clay (altered fspr?)	subangular
		2	100.00	60.00	Quartz	subangular
		3	250.00	200.00	Clay (altered glass?)	subangular
		4	30.00	30.00	Quartz	angular
		5	75.00	50.00	Quartz	angular
		6	100.00	50.00	Clay (altered glass?)	angular
		7	200.00	100.00	Clay (altered glass?)	angular
		8	50.00	30.00	Quartz	angular
		9	90.00	80.00	Clay (altered glass?)	angular
		10	120.00	80.00	Clay (altered glass?)	angular

		11	20.00	20.00	Quartz	subangular
		12	75.00	30.00	Glass	angular
		13	50.00	50.00	Quartz	subangular
		14	50.00	50.00	Quartz	angular
		15	100.00	50.00	Quartz	angular
		16	120.00	120.00	Clay (altered grain)	subrounded
		17	50.00	40.00	Clay (altered grain)	angular
		18	60.00	50.00	Quartz	angular
		19	25.00	20.00	Chromium oxide	
		Average	**86.32**	**61.05**		

General notes on UHA2.5: Quartz, glass, Cr oxides, and a lot of probable glass/ash.
Did whole-stub SEM photo of stub 4-- at ~40X magnification.

UHA	2.9	1	90	80	Quartz	angular
		2	200	100	Clay (altered grain)	subangular
		3	250	150	Quartz	angular
		4	125	125	Clay (altered grain)	angular
		5	100	75	Clay (altered grain)	subrounded
		6	100	100	Clay (altered grain)	subrounded
		7	125	100	Clay (altered grain)	subrounded
		8	75	75	Clay (altered grain)	subrounded
		Average	**133.13**	**100.63**		

General notes on UHA2.9: Plentiful altered clay, but lots of tiny angular quartz (5-10μm); chemistry on the clay material looks just like that on the others, w/ high Ti.

UHA	3.9	smear				Clay
		1	40	20.00	Quartz	Angular

General notes on UHA3.9: Is a smear of exclusively clays (probably altered ash?)

UHA	4.7	1	250	150	Clay (altered grain)	subangular
		2	250	150	Clay (altered grain)	subangular
		3	600	500	Clay (altered grain)	subangular
		4	150	100	Clay (altered grain)	subangular
		5	200	100	Clay (altered grain)	subangular
		Average	**290.00**	**200.00**		

General notes on UHA 4.7: a lot of what looks like altered clay, just like grains in UHA12.9; several "grains" that have since disintegrated on the stub-- v. fragile.

UHA	4.9	1	120.00	120.00	?	mini droplet

UHA	6.3	1	125	125	Clay (altered grain)	subrounded
		2	125	100	Rock fragment	subangular
		Average	**125.00**	**112.50**		

General notes on UHA6.3: doesn't have the a lot of altered clay.

UHA	7.9	1	1400	1000	qtz/alb/kspr	angular
		2	260	160		subangular
		3	330	230	rock frag	subangular
		4	500	300	qtz/kspr, clay?	subangular
		5	475	225		angular
		6	300	250	qtz/kspr/alb	very angular
		7	270	190	qtz	angular
		8	650	300	plag (An30)	very angular
		Average	**523.13**	**331.88**		

UHA	9.7	1	150	75	Quartz w/clay	angular
		2	100	100	Quartz	angular
		3	250	100	Alk fspar	angular
		Average	**166.67**	**91.67**		

General notes on UHA9.7: doesn't have a lot of altered clay.

UHA	10.5	1	325	150	Quartz	angular
		2	300	200	Quartz	angular
		3	250	200	Quartz	rounded
		4	250	200	Clay (altered glass?)	angular
		5	200	175	Quartz	angular
		6	300	200	Quartz	subangular
		7	200	200	Quartz	subrounded
		8	175	175	Quartz	subrounded
		9	100	100	Quartz	subangular
		10	175	100	Clay (altered glass?)	angular
		11	75	75	Quartz	subangular
		12	50	50	Quartz	subangular
		Average	**200.00**	**152.08**		

General notes on UHA10.5: Does not have a lot of altered clay; several grains, but all are authigenic quartz growing on what appears to be "spongey" very pitted quartz. Hypothesis-- these grains are quartz psuedomorphing pumice? But in other samples we've seen what we think is pumice altered to clay. So in the case of these, where did the Al go?

UHA	11.7	1	200	75	Clay (altered grain)	subangular
		2	100	100	Clay (altered grain)	subangular
		3	150	125	Clay (altered grain)	subangular
		4	150	150	Clay (altered grain)	subangular
		5	100	75	Clay (altered grain)	subrounded
		6	25	20	Quartz	angular
		7	75	75	Quartz	angular

		Average	**114.29**	**88.57**		

General notes on UHA11.7: similar to above-- smeared fine-grained material plus a few "grains" that are disintegrating. Presence of minor quartz (also reinforcing the volcanic interpretation).

UHA	11.7	1	500	200	Clay (altered grain)	subangular
		2	430	210	Clay (altered grain)	subrounded
		3	320	210	clay coated qz	subangular
			416.666	**206.666**		
		Average	**7**	**7**		
UHA	12.1	1	100	75	Clay (altered grain)	subangular
		2	75	50	Clay (altered grain)	subangular
		3	30	30	Quartz	angular
		Average	**68.33**	**51.67**		
UHA	12.9	1	500	300	Clay (altered grain)	subangular
		2	500	300	Clay (altered grain)	subangular
		3	300	250	Clay (altered grain)	subangular
		4	250	250	Clay (altered grain)	subangular
		5	300	200	Clay (altered grain)	subangular
		6	500	300	Clay (altered grain)	subangular
		7	400	250	Clay (altered grain)	subangular
		8	300	250	Clay (altered grain)	subangular
		9	300	250	Clay (altered grain)	subangular
		10	250	100	Clay (altered grain)	subangular
		11	400	350	Clay (altered grain)	subangular
		12	250	200	Clay (altered grain)	subangular
		13	300	250	Clay (altered grain)	subangular
		14	400	400	Clay (altered grain)	subangular
		15	300	200	Clay (altered grain)	subangular
		16	200	200	Clay (altered grain)	subangular
		17	500	300	Clay (altered grain)	subangular
		18	500	300	Clay (altered grain)	these are grains that appear to have been crushed (since mounting), so were v fragile
		19	700	300	Clay (altered grain)	these are grains that appear to have been crushed (since mounting), so were v fragile
		20	600	400	Clay (altered grain)	these are grains that appear to have been crushed (since

						mounting), so were v fragile
		21	400	400	Clay (altered grain)	subangular
		22	300	250	Clay (altered grain)	subangular
		Average	**384.09**	**272.73**		
UHA	12.9	2	240	190	Clay or Kspar (altered grain)	Subrounded
		3	500	350	Clay (altered grain)	Subangular
		4	220	175	Clay (altered grain)	Subangular
		5	200	200	Clay (altered grain)	Rounded
		6	330	200	Clay (altered grain)	Subangular
		7	375	200	Clay (altered grain)	Subangular
		8	240	120	Clay (altered grain)	Subangular
		9	400	180	Clay (altered grain)	Angular
		10	430	200	Clay (altered grain)	angular
		11	310	200	Clay (altered grain)	Angular
		12	200	140	Clay (altered grain)	subrounded
		13	100	75	Clay (altered grain)	subangular
		14	70	55	Clay (altered grain)	Subrounded
		15	210	100	Clay (altered grain)	Subangular
		16	90	70	qz	Subangular
		17	200	100	Clay (altered grain)	Angular
		18	350	210	Clay (altered grain)	Subangular
		19	150	80	Clay (altered grain)	Subangular
		20	180	100	Clay (altered grain)	Subangular
		21	250	200	Clay (altered grain)	Subangular
		Average	**252.25**	**157.25**		
UHA	13.5	1	75	75	Clay (altered grain)	subrounded
		2	80	70	Clay (altered grain)	subrounded
		3	100	70	Clay (altered grain)	subrounded
		4	110	70	Clay (altered grain)	subrounded
		5	60	40	Clay (altered grain)	subrounded
		6	100	100	Clay (altered grain)	subrounded
		7	80	80	Clay (altered grain)	subrounded
		Average	**86.43**	**72.14**		
General notes on UHA13.5: A lot of altered clay, with a few larger "grains" composed of altered clay						
UHA	15.2-15.3	1	20	20.00	Kspar (OR92, AL7)	subangular
		2				
UHA	21.9+21.6	1	350	200	qtz/kspr/biot	subrounded
		2	?	?	glass	
		3	400	250	qtz	

		Average	**375.00**	**225.00**		
MNE	6.1	1	900.00	700.00	kspr/plag/hbl	subrounded
MNE	9.3	1	1200	1000	qtz/plag/kspr	very angular
		2	850	450	plag/kspr	angular
		3	480	300	plag	angular
		4	400	275	plag	subangular
		5	400	325	plag/kspr/hbl	very angular
		6	300	170	qtz	very angular
		7	300	160	qtz-dom'd	subangular
		8	250	175	qtz	rounded
		9	275	200	alb/kspr	very angular
		10	450	310	qtz/plag/kspr?	subangular
		11	460	270	qtz/plag	subrounded
		12	450	275	plag	very angular
		13	700	600	kspr? Clay coat?	subrounded
		14	550	350	kspr/plag	rounded
		Average	**504.64**	**347.14**		
MNE	11.6	1	410.00	275.00	qtz	subangular
MNE	13.1	1	500	375	qtz/kspr/plag	very angular
		2	300	280	qtz+	subrounded
		3	400	200	qtz	very angular
		4	400	240	qtz/kspr	subangular
		5	390	250	kspr	subangular
		6	620	300	alb	very angular
		7	330	260	qtz/kspr/Na plag, Mag	subangular
		8	750	540	alb/plag	subangular
		Average	**461.25**	**305.63**		
MNE	11.1	1	530	340	qtz	subangular
		2	400	250	qtz	angular
		3	500	250	plag	angular
		4	180	170	qtz	rounded
		5	375	250	qtz	very angular
		6	650	400	qtz/alb	subangular
		7	550	210	hbl	very angular
		8	400	200	qtz	very angular
		9	500	340	plag (An 35-40)	very angular
		10	370	330	qtz/hbl	subangular
		11	350	250	biot	angular
		12	250	250	plag	very angular

13	290	140	qtz	very angular
14	575	340	qtz	very angular
15	540	380	kspr/plag/hbl/alb	subangular
16	180	90	qtz	rounded
17	430	240	glass (rhyolite?)	angular
18	410	340	plag	very angular
19	550	240	glass (rhyolite)?	very angular
20	700	500	qtz/hbl	very angular
21	550	500	clay-coated qtz?	angular
22	390	200	spalled clay coat	angular
23	500	370	mostly plag	subangular
24	300	150	hbl/plag/alb	very angular
25	250	225	qtz	very angular
26	380	210	qtz	very angular
27	530	200	qtz/hbl	very angular
28	700	530	hbl/plag/kspr	subangular
29	340	330	qtz/plag	angular
30	270	250	hbl	very angular
31	250	240	hbl/biot	very angular
32	390	275	plag/hbl	angular
33	310	290	plag (An 43)	subangular
34	360	230	qtz	angular
35	170	110	qtz	very angular
36	190	160	qtz	subrounded
37	210	180	qtz	angular
38	210	125	qtz	angular
39	225	150	qtz	very angular
40	750	350	plag	very angular
41	310	210	qtz/plag	subangular
42	500	310	qtz	very angular
43	275	160	plag	very angular
44	350	290	qtz	very angular
45	500	330	qtz/plag	subangular
46	180	115	qtz	rounded
47	300	210	plag	very angular
48	220	160	qtz/plag	very angular
49	180	150	qtz	rounded
50	410	180	plag	very angular
51	300	200	hbl	subangular
52	260	200	hbl/plag	very angular
53	500	275	qtz/hbl	very angular
54	470	300	glass (rhyolite)?	very angular
55	250	140	plag	very angular
Average	**382.00**	**251.18**		

MNE	11.1	1	1247	782	plag/qtz/kspr/musc/garn/epid	
		2	1129	1129	qtz/plag (An15)/mag	
		3	1215	1215	qtz/plag(An15)/hbl	
		4			hbl/ternary plag (An9 Or11, Al)	
		5	300	300	pla(An5-20)	
		6	800	80	alb/hbl	
		7	632	632	plag (An30)	
		8	500	300	sodic plag/hbl	
		9	1000	800	qtz/ternary plag	
		10	1000	800	plag (An25-30)/qtz	
		11	700	350	epidote	
		12	1053	800	sodic plag/hbl	
		Average	**870.55**	**653.45**		

GH3	0.0-0.1	1	200	150	Quartz	biprismal
		2	100	75	rock fragment	subangular
		3	150	100	Quartz	subangular
		4	150	100	Quartz	subangular
		5	150	100	Quartz	rounded
		6	150	100	Quartz	subangular
		7	200	150	Quartz	
		8 to 11			Quartz	subangular
		12	200	100	Quartz	rounded
		13	200	100	Quartz	rounded
		14	150	150	Rock fragment	subangular
		15 to 18	150	100	Quartz	subangular
		19	150	150	Quartz	rounded
		20	100	100	Quartz	rounded
		20 to 25	120	100	Quartz	subangular
		Average	**155.00**	**112.50**		

GH3	0.5	1	650	300	Quartz	euhedral
		1 to 17	up to 600	300	Quartz	euhedral
		13	600	350	Quartz	euhedral
		Average	**616.67**	**316.67**		

This sample is entirely authigenic prisms of quartz-- w/ spongy interiors and carapaces of euhedral quartz; one w/ opal interior.

GH3	0.7	1	125	100	Glass?	subangular
		2	150	100	Quartz	subangular
		3	100	75	Pumice	subangular
		4	100	75	Pumice	subangular
		5	300	100	Pumice	subangular
		6	200	100	Pumice?	subangular

		7	100	75	Pumice?	subangular
		Average	**153.57**	**89.29**		

Note that the "smeared" area turns out to consist of what is probably pumice-- highly friable spongy material. So when we see spongy quartz, it must be the "end result" of alteration of these glasses.

GH3	1.1	1	500	300	Qz	Subangular
			200	125		
GH3	2.2	1	100	90	Qz (with clay/Si coating)	Subrounded
		2	200	125	Anorthite	Angular
		3	200	125	Microcline	Subrounded
		4	1250	1000	Qz (with clay/Si coating)	Subrounded
		5			Anorthoclase(maybe glass)	Subangular
		6				
		Average	**390**	**293**		
GH3	2.5	1	200	125	Pumice	angular
		2	100	75	Pumice?	subrounded
		3	75	50	Fe-Cr oxide	subangular
		4	300	75	Silica	angular
		Average	**168.75**	**81.25**		
GH3	3	1	250	70	Qz	Subangular
		2	300	225	Qz	Angular
		3	240	125	Qz	Subangular
		4	100	125	Qz	Subangular
		Average	**222.50**	**136.25**		
GH3	5.9	1	350	75	Quartz	euhedral
		2	150	100	Quartz	euhedral
		3	275	75	Quartz	euhedral
		4	100	75	Quartz	angular
		5	250	100	Quartz	subeuhedral
		Average	**225.00**	**85.00**		

General notes on GH3 5.9: all are whole (or pieces of) quartz prisms (authigenic)-- but all VERY spongey.

GH3	6.1	1	100	75	Kspar	subangular
		2	200	150	Qtz+Clay	subangular
		3	75	75	Quartz	subangular
		4	75	75	Quartz	angular
		5	100	60	Quartz	angular

		6	50	40	Quartz	euhedral
		7	100	75	Quartz	euhedral
		8	250	75	Quartz	subangular
		9	50	40	Quartz	angular
		10	50	50	Quartz	angular
		11 to 20				
		11	100	80	Kspar+Qtz	
		12	225	100	Quartz	euhedral
		13	150	80	Quartz	subangular
		14	150	80	Quartz	subangular
		15	100	80	Quartz	subangular
		16	100	80	Quartz	subangular
		17	70	50	Quartz	subangular
		18	175	100	Quartz	subangular
		19	120	120	Quartz+Clay	subangular
		20	100	100	Quartz	subangular
		21	75	50	Albite	subangular
		22	120	80	Quartz	angular
		23	150	100	Kspar	subangular
		24 to 41				
		24	100	100	Quartz	subangular
		25	120	75	Quartz	subangular
		26	60	50	Quartz	angular
		27	220	175	Kspar	subrounded
		28	100	75	Quartz	subangular
		29	75	75	Quartz	subangular
		30	125	75	Quartz	subangular
		31	75	50	Quartz	subangular
		32	75	50	Qtz+Clay	subangular
		33	50	50	Quartz	subrounded
		34	60	50	Quartz+Kspar	subrounded
		35	100	70	Quartz	subangular
		36	75	70	Quartz	subangular
		37	200	100	Quartz	euhedral
		38	125	125	Quartz	equant
		39	120	120	Quartz	
		40	150	100	Quartz	subrounded
		41	125	100	Kspar	equant
		42-52-- all look like authigenic on spongey quartz, of sizes in 50-100 µm range				
		Average	**113.17**	**81.10**		

General notes on GH3 6.1: See both the authigenic prisms, and the overgrown spongey quartz-- not sure what the precursors were.

GH3	6.9	1	200	200	Quartz	subangular
		2	200	200	Quartz	subrounded

		3	200	100	Quartz	subangular
		4	100	75	Quartz	subrounded
		5	100	75	Quartz+sanidine	subrounded
		6	200	100	Quartz + glass	rounded
		7 to 22	150	100	Quartz	
		23 to 27	200	100	Quartz	subangular
		Average	**168.75**	**118.75**		
GH3	7.1	1	300	300	Quartz	subrounded
		2	100	100	Quartz	subrounded
		3	100	75	Quartz	rounded
		4	150	100	Glass	rounded
		5	150	100	Glass	rounded
		6	150	100	Glass	subrounded
		7	150	100	Quartz	
		8	100	75	Glass	subrounded
		Average	**150.00**	**118.75**		

Lots of rounded-looking glass -- in some cases altering to clay coatings; can locally see hexagonal plates of clays (kaolinite) on surfaces

GH3	7.7	1	300	250	Plagioclase	angular
		2	200	100	Quartz	subangular
		3	200	100	Sanidine	
		4 to 10	200	100	Quartz	subrounded
		11	150	150	Biotite w/ Qtz	subangular
		12 to 18	200	100	Quartz	subrounded
		19 and 20	75	50	Kspar	subangular
		19 to 31	200	100	Quartz	subrounded
		32	50	50	Cr-rich iron oxide	
		32 to 41	100	75	Quartz	subangular
		42	50	50	Rutile	
		43	150	100	Kspar	subrounded
		42 to 50			Quartz	
		Average	**156.25**	**102.08**		
GH3	7.9	1	1000	300	authigenic prism	euhedral
		2	1000	300	authigenic prism	euhedral
		3	500	200	authigenic prism	euhedral
		4	500	300	authigenic prism	euhedral
		5	500	300	authigenic prism	euhedral
		6	500	300	authigenic prism	euhedral
		7	300	200	authigenic prism	euhedral
		8	300	200	authigenic prism	euhedral

		9	300	200	authigenic prism	euhedral
		10	150	150	quartz	rounded
		11	75	50	spongey quartz	subangular
		12	150	120	quartz	rounded
		13	500	250	authigenic prism	euhedral
		14	300	300	authigenic prism	euhedral
		15	500	300	authigenic prism	euhedral
		16	300	200	authigenic prism	euhedral
		Average	**429.69**	**229.38**		
GH3	9.1	1	150	125	Quartz	subrounded
		2	350	250	Quartz	subangular
		3	200	150	Quartz	subrounded
		4	125	125	Quartz	subrounded
		5	125	125	Quartz	subrounded
		6 to 12	200	150	Quartz	subrounded
		10	150	125	Quartz	subrounded
		13 to 19	125	100	Quartz	subangular
		20 to 21	200	150	Quartz	
		20	200	150	Quartz	subangular
			200	150	Quartz	rounded
		21 to 30	100	75	Quartz	subangular
		31	125	100	Sanidine	angular
		32-41	up to 150	50	Quartz	subangular
		41	25	25	Titanite	subangular
		42	250	200	Rock Frag	subangular
		43 to 44	150	150	Quartz	subangular
		45 55	150	125	Quartz	subangular
		56	75	75	Sanidine	subrounded
		57 to 61	up to 200	100	Quartz	subangular
		Average	**162.50**	**125.00**		

Mostly spongy quartz with minor authigenic overgrowths; seemed a bit more rounded than others.

GH3	9.5	1	300	100	authigenic prism	euhedral
		2	225	150	authigenic prism	euhedral
		3	150	150	spongey quartz	subangular
		4	175	125	spongey quartz	subangular
		5	150	100	spongey quartz	subangular
		6	200	200	spongey quartz	subangular
		7	100	100	rock fragment	subangular
		8	200	125	spongey quartz	subangular
		9	200	150	spongey quartz	subangular
		10	125	100	spongey quartz	subangular

		11	150	100	spongey quartz	subangular
		12	150	40	authigenic prism	euhedral
		13	200	100	spongey quartz	angular
		14	75	75	spongey quartz	subrounded
		Average	**171.43**	**115.36**		
GH3	9.9	1	200	125	spongey prism	angular
		2	75	75	spongey kspar+silica	angular
		3	150	100	spongey quartz	angular
		4	75	75	spongey quartz	angular
		5	150	75	spongey quartz	angular
		6	200	100	spongey quartz	angular
		7	150	100	spongey quartz	subangular
		8	150	100	spongey quartz	subangular
		9	100	75	spongey quartz	subangular
		10	125	75	spongey prism	subangular
		11	200	125	spongey quartz	subangular
		12	125	100	spongey quartz	subangular
		13	200	125	spongey quartz	subangular
		14	100	100	spongey quartz	subangular
		15	200	75	spongey quartz	subangular
		16	75	75	spongey quartz	subangular
		17	100	75	spongey quartz	subangular
		18	100	75	spongey quartz	subangular
		19	100	75	spongey quartz	subangular
		20	100	100	glass	bubble walls
		Average	**133.75**	**91.25**		
GH3	11.7	1	150	150	Quartz	subangular
		2	125	75	Kspar	rounded
		3	75	50	Quartz	subangular
		4	250	200	Quartz	subangular
		Average	**150.00**	**118.75**		
GH3	12.9	1	275	250	rock fragment	angular
		2	500	75	spongey quartz	auth prism
		3	100	100	spongey quartz	subangular
		4	200	150	spongey quartz	angular
		5	150	75	spongey quartz	subangular
		6	200	200	spongey quartz	angular
		7	125	75	spongey quartz	subangular
		8	300	175	glass	angular
		9	200	125	spongey quartz	subangular

		10	75	75	spongey quartz	subangular
		11	200	150	spongey quartz	subangular
		12	75	75	spongey quartz	subangular
		13	200	100	rock fragment	subangular
		14	200	100	spongey quartz	subangular
		15	100	100	rock fragment	subrounded
		16	100	100	rock fragment	subrounded
		17	100	100	rock fragment	subrounded
		18	50	50	Ca-plagioclase	angular
		19	200	150	spongey quartz	subangular
		20	200	150	etched quartz	subangular
		Average	**177.50**	**118.75**		

Did whole-stub SEM photo of stub 42-- at ~40X magnification.

GH3	13.5	1	100	75	rock fragment	angular
		2	100	75	spongey quartz	subrounded
		3	125	100	spongey quartz	subrounded
		4	100	75	spongey quartz	subrounded
		5	100	75	spongey quartz	subrounded
		6	125	100	spongey quartz	subrounded
		7	50	30	spongey quartz	subangular
		8	70	50	spongey quartz	subrounded
		9	50	50	spongey quartz	subrounded
		10	200	100	spongey quartz	subangular
		11	75	35	spongey quartz	subrounded
		12	200	100	spongey quartz w/ biotite	subangular
		13	100	75	spongey quartz	subangular
		14	125	75	spongey quartz	subangular
		15	200	100	spongey quartz	subrounded
		16	100	75	spongey quartz	subangular
		Average	**113.75**	**74.38**		

GH3	13.9	1 to 4	up to 400	175	Quartz	euhedral
		5 to 6	up to 125		Quartz	subangular
		7 to 10	up to		Quartz	subangular
		10	125	75	Quartz	subangular
		11			Quartz	subangular
		12 to 16	200	100	Quartz	subangular
		17	150	75	Quartz	euhedral
		18 to 24	up to 150	100	Quartz	subangular
		25 to 28	175	100	Quartz	euhedral

		29	125	100	Quartz	rounded
		30 to 31	150	100	Quartz	euhedral
		32	100	100	Quartz	subangular
		Average	**175.00**	**102.78**		
Mostly spongy quartz w/ minor authigenic growths						
GH3	14.1	1	200	125	Rock Frag	angular
		2	200	125	Quartz	angular
		3	200	150	Frag?	subangular
		4	100	100	Quartz	subangular
		Average	**175.00**	**125.00**		
GH3	14.9	1	300	75	authigenic prism	euhedral
		2	150	100	spongey quartz	angular
		3	150	120	spongey quartz	subangular
		4	200	100	spongey quartz	subangular
		Average	**200.00**	**98.75**		
GH3	15.5	1	200	150	spongey quartz	subrounded
		2	200	100	spongey quartz	subangular
		3	150	125	spongey quartz	subrounded
		4	150	125	spongey quartz	subrounded
		5	100	100	spongey quartz	subangular
		6	150	125	spongey quartz	subangular
		7	150	150	spongey quartz	subangular
		8	150	125	spongey quartz	subangular
		9	150	125	spongey quartz	subangular
		10	150	125	spongey quartz	subangular
		11	150	125	spongey quartz	subangular
		12	150	125	spongey quartz	subangular
		13	50	50	spongey quartz	subangular
		14	150	125	spongey quartz	subangular
		15	125	125	spongey quartz	subangular
		16	125	125	spongey quartz	subangular
		17	125	125	spongey quartz	subangular
		18	125	125	spongey quartz	subangular
		19	125	125	spongey quartz	subangular
		20	250	150	spongey quartz	subangular
		21	150	125	spongey quartz	subangular
		22	150	125	spongey quartz	subangular
		23	125	125	spongey quartz	subangular
		24	125	125	spongey quartz	subangular
		25	125	125	spongey quartz	subangular
		26	125	125	spongey quartz	subangular

		27	125	125	spongey quartz	subangular
		28	125	125	spongey quartz	subangular
		29	125	125	spongey quartz	subangular
		30	200	100	spongey quartz	subangular
		31	125	125	spongey quartz	subangular
		32	75	75	spongey quartz	auth prism
		33	100	75	spongey quartz	subangular
		34	200	200	spongey quartz	subangular
		35	150	150	spongey quartz	subangular
		36	150	150	spongey quartz	subangular
		37	150	150	spongey quartz	subangular
		38	200	200	spongey quartz	subangular
		39	75	75	spongey quartz	subrounded
		40	100	100	spongey quartz	subrounded
		41	125	125	spongey quartz	subrounded
		42	100	75	spongey quartz	prism piece
		43	100	50	spongey quartz	prism piece
		44	75	75	spongey quartz	subrounded
		45	100	100	spongey quartz	subrounded
		46	200	150	spongey quartz	subangular
		47	100	100	spongey quartz	subangular
		48	50	50	spongey quartz	subangular
		49	75	100	spongey quartz	subangular
		50	75	50	spongey quartz	subangular
		51	75	50	spongey quartz	subangular
		52	125	75	spongey quartz	subangular
		53	125	100	spongey quartz	subangular
		Average	**131.13**	**114.62**		
GH3	16.1	1 to 10	100	75	Quartz	subangular
		10	100	75	Rock Frag	subangular
		11 to 19	up to 150	50	Quartz	subangular
		19	125	125	Quartz	rounded
		20 to 43	up to 200	50	Quartz	subangular
		43	150	125	Rock Frag	subangular
		44-55	up to 150	50	Quartz	subangular
		56	40	25	Zircon	equant
		57	60	40	Rock Frag	subangular
		58 to 74	up to 200	50	Quartz	subangular
		74	100	100	Quartz	rounded

		75 to 80	up to 150	50	Quartz	subangular
		81 to 85	up to 150	50	Quartz	subangular
		86	150	125	Kspar	subrounded
		87	50	50	Hematite	angular
		88 to 98	100	75	Quartz	subangular
		Average	**123.44**	**69.69**		
Mostly spongy quartz with minor overgrowths, but some zircons						
GH3	16.3	1	225	200	spongey quartz	subrounded
		2	200	125	spongey quartz	subrounded
		3	150	125	spongey quartz	subrounded
		4	250	125	spongey quartz	subrounded
		5	200	100	spongey quartz	subrounded
		6	300	150	spongey quartz	subrounded
		7	50	25	spongey quartz	subangular
		8	150	100	kspar	subangular
		9	125	100	spongey quartz	subangular
		10	150	125	spongey quartz	subangular
		11 to 23	150 to 75			
		Average	**180.00**	**117.50**		
GH3	17.3	1	125	100	spongey quartz	subangular
		2	125	100	spongey quartz	subangular
		3	125	100	spongey quartz	subangular
		4	125	100	spongey quartz	subangular
		5	125	100	spongey quartz	subangular
		6	125	100	spongey quartz	subangular
		7	125	100	spongey quartz	subangular
		8	125	100	spongey quartz	subangular
		9	125	100	spongey quartz	subangular
		10	125	100	spongey quartz	subangular
		11	125	100	spongey quartz	subangular
		12	125	100	spongey quartz	subangular
		13	200	175	spongey quartz	subangular
		14	200	150	spongey quartz	subrounded
		15	250	100	spongey quartz	subangular
		16	100	100	spongey quartz	subrounded
		17	100	100	spongey quartz	subangular
		18	100	100	spongey quartz	subrounded
		19	200	125	spongey quartz	subrounded
		20	150	125	spongey quartz	subangular

		21	175	100	spongey quartz	subangular
		22	175	100	spongey quartz	subangular
		23	75	65	kspar	subrounded
		Average	**140.22**	**106.09**		
GH3	18.1	1	50	50	Quartz?	subangular
		2	40	40	Quartz?	subangular
		3	100	75	Quartz	subangular
		4	125	100	Quartz	subangular
		5 to 6	125	125	Quartz	subrounded
		7 to 9	100	100	Quartz	subrounded
		10	125	125	Quartz	subangular
		11 to 20	100-200	100-200	Quartz	subangular
		21 to 40			Quartz	subangular
		30	50	50	Kspar	rounded
		41-60	100ish	50ish	Quartz	subangular
		61	600	300	Rock Frag (volc)	angular
		62-100	100-200	50ish	Quartz	subangular
		Average	**142.92**	**101.25**		

All grains seem to be on their way to becoming recrystallized quartz. All look to be volcanic except for one possible eolian (the kspar).

GH3	18.5	1 to 6	150		Quartz	subangular
		6	150	125	Glass? Clay?	
		8	250	150	Clay?	subrounded
		9 to 12	150	75	Quartz	subangular
		13 to 26	up to 250	50	Quartz	subangular
		27 to 30	150	100	Quartz	subangular
		31	50	40	Glass	angular
		32	150	100	Silica	subrounded
		33 to 86	up to 200	50	Quartz	subangular
		86	75	75	Quartz	angular
		87 to 99	up to 150	50	Quartz	subangular
		Average	**156.82**	**81.50**		

Mostly spongy quartz with local authigenic overgrowths, some denser quartz (phenocrysts?), one definitive ash fragment

GH3	19.3	1	100	75	quartz	subrounded
		2	150	100	spongey quartz	subangular
		3	100	75	spongey quartz	subangular
		4	200	100	spongey quartz	subangular
		5	100	75	quartz	angular

		6	125	100	spongey quartz	subangular
		7	50	25	spongey prism	subangular
		8	100	50	spongey quartz	subangular
		9	125	100	spongey quartz	subangular
		10	100	75	spongey quartz	subangular
		Average	**115.00**	**77.50**		
	19.3					
GH3	(cont.)	1 to 4	150	100	Quartz	subangular
		5 to 18	up to 250	75	Quartz	subangular
		19	225	125	Glass	subangular
		20	150	100	Quartz	subangular
		21	300	150	Quartz	euhedral
		24 to 41	150	75	Quartz	subangular
		Average	**204.17**	**104.17**		

Mostly spongy quartz with local authigenic overgrowths

GH3	19.5	1	300	125	Quartz	euhedral
		2	300	125	Quartz	euhedral
		3	450	150	Quartz	euhedral
		4	150	100	Quartz	subangular
		5	200	150	Quartz	angular
		6	150	50	Quartz	angular
		7	100	75	Quartz	subangular
		8	150	100	Quartz	subangular
		9	200	100	Quartz	euhedral
		10	100	50	Quartz	subangular
		11 to 15	100	50	Quartz	subangular
		16 to 23	150	50	Quartz	subangular
		24 to 33	100	50	Quartz	subangular
		Average	**188.46**	**90.38**		

Theme in this sample is authigenic quartz growing on spongy, and biprisms of quartz (presumably the end product of recrystallization).

GH3	20.1	1	150	100	perthitic kspar	angular
		2	100	75	spongey quartz	subrounded
		Average	**125.00**	**87.50**		
GH3	21.9	1&2	100	100	spongey quartz	subangular
		3, 4, 5	50	50	spongey quartz	subrounded
		6	200	150	spongey quartz	subangular
		7, 8	150	100	spongey quartz	subangular
		9, 10, 11	150	100	spongey quartz	subangular

		12	150	100	spongey quartz	subangular
		13	150	100	spongey quartz	subangular
		14, 15	150	75	kspar on SQ	subangular
		16, 17, 18	100	75	spongey quartz	subangular
		19	75	50	rounded	kspar
		20,21,22	150	100	spongey quartz	subangular
		23	100	100	spongey quartz	subangular
		24	100	50	spongey quartz	angular
		25	150	125	spongey quartz	subangular
		26	150	75	spongey quartz	subangular
		Average	**128.33**	**90.00**		
GH3	22.5	1 to 3	up to 400	100	Quartz	euhedral
		4 to 6	250	50	Quartz	euhedral
		7	200	100	Quartz	euhedral
		8 to 13	60	40	Quartz	subangular
		14 to 22	250	50	Quartz	subangular
		21	100	75	Kspar	subrounded
		23 to 24	200	150	Quartz	subangular
		25	200	150	Quartz	euhedral
		26	100	60	Pumice	angular
		27 to 29	50	50	Quartz	subangular
		30 to 32	200	50	Quartz	subangular
		33 to 38	up to 400	100	Quartz	subangular
		39-48	up to 300	100	Quartz	subangular
		49 to 60	up to 400	75	Quartz	subangular
		60	150	125	Sodic Orthoclase	rounded
		61 to 71	up to 500 (most 75)	50	Quartz	subangular
		Average	**235**	**82.8125**		

Theme here is lots of the biprismal quartz, pieces thereof, and authigenic quartz growing on spongy.

GH2	0.8	1	125	100	qz	subangular
GH2	1	1	206	132	qz	diagenetic
		2	185	115	qz	subrounded
		3	213	68	qz	angular
		4	121	85	qz	subangular

		5	132	64	qz	diagenetic
		6	138	47	qz	subangular
		7	85	85	plag(albite)	rounded
		8	106	89	qz	angular
GH2	1.1	1	261	207	diagenetic qz	doubly terminated
		2	176	106	diagenetic qz	doubly terminated
		3	144	85	diagenetic qz	doubly terminated
GH2	1.7	1	356	106	diagentic qz	doubly terminated
		2	239	207	qz	subangular
		3	239	197	diagentic qz	doubly terminated
		4	771	255	diagentic qz	doubly terminated
		5	500	202	diagentic qz	doubly terminated
		6	649	277	diagentic qz	doubly terminated
		7	261	223	qz	subangular
		8	271	170	diagentic qz	doubly terminated
		9	378	181	diagentic qz	doubly terminated
		10	207	160	qz	subrounded
		11	80	74	qz	angular
		12	144	90	microcline	subrounded
		13	112	74	diagentic qz	doubly terminated
		14	101	74	qz	diagenetic
		15	74	74	qz	rounded
		16	160	85	diagentic qz	doubly terminated
		17	90	74	qz	subangular
		18	101	69	Iron Oxide	angular
		19	96	74	qz	subrounded
		20	186	80	diagentic qz	doubly terminated
GH2	2.2	1	229	113	qz	Angular
		2	218	207	qz	diagenetic
		3	308	303	qz	diagenetic
		4	207	90	qz	angular
		5	229	117	qz	Sub angular
		6	144	90	qz	sub rounded
		7	234	133	qz	sub angular
		8	106	90	qz	diagenetic
		9	399	287	qz	sub rounded
GH2	2.3	1	888	346	diagenetic qz	doubly terminated
		2	718	218	diagenetic qz	doubly terminated
		3	335	138	diagenetic qz	doubly terminated
		4	319	112	diagenetic qz	doubly terminated
		5	362	128	diagenetic qz	doubly terminated

		6	378	122	diagenetic qz	doubly terminated
		7	686	287	diagenetic qz	doubly terminated
		8	479	160	diagenetic qz	doubly terminated
		9	676	255	diagenetic qz	doubly terminated
		10	245	186	diagenetic qz	doubly terminated
		11	122	74	diagenetic qz	doubly terminated
		12	149	128	diagenetic qz	doubly terminated
		13	346	165	diagenetic qz	doubly terminated
		14	213	144	diagenetic qz	doubly terminated
		15	367	112	diagenetic qz	doubly terminated
		16	298	160	diagenetic qz	doubly terminated
		17	298	144	diagenetic qz	doubly terminated
		18	144	85	diagenetic qz	doubly terminated
		19	324	112	diagenetic qz	doubly terminated
		20	117	74	diagenetic qz	doubly terminated
GH2	2.6	1	920	298	diagenetic	Doubly Terminated qz
		2	888	293	diagenetic	Doubly Terminated qz
		3	628	404	diagenetic	Doubly Terminated qz
		4	399	186	diagenetic	Doubly Terminated qz
		5	723	213	diagenetic	Doubly Terminated qz
		6	303	128	diagenetic	Doubly Terminated qz
GH2	2.7	1	622	239	diagenetic qz	Doubly Terminated
		2	718	229	diagenetic qz	Doubly Terminated
		3	521	356	diagenetic qz	Doubly Terminated
		4	559	207	diagenetic qz	Doubly Terminated
		5	532	261	diagenetic qz	Doubly Terminated
		6	622	229	diagenetic qz	Doubly Terminated
		7	574	191	diagenetic qz	Doubly Terminated
		8	638	218	diagenetic qz	Doubly Terminated
		9	564	207	diagenetic qz	Doubly Terminated
		10	553	133	diagenetic qz	Doubly Terminated
		11	101	85	qz	angular
		12	372	186	diagenetic qz	Doubly Terminated
		13	261	144	diagenetic qz	Doubly Terminated
		14	532	223	diagenetic qz	Doubly Terminated
		15	154	96	qz	angular
		16	213	149	diagenetic qz	Doubly Terminated
		17	144	101	qz	subrounded
		18	106	59	diagenetic qz	Doubly Terminated
		19	170	138	qz	subrounded
		20	176	149	qz	diagenetic
GH2	2.8	1	426	186	diagenetic qz	doubly terminated

		2	404	202	diagenetic qz	doubly terminated
		3	335	122	diagenetic qz	doubly terminated
		4	410	170	diagenetic qz	doubly terminated
		5	314	101	diagenetic qz	doubly terminated
		6	340	122	diagenetic qz	doubly terminated
		7	362	149	diagenetic qz	doubly terminated
		8	309	122	diagenetic qz	doubly terminated
		9	340	106	diagenetic qz	doubly terminated
		10	282	117	diagenetic qz	doubly terminated
		11	96	96	qz	rounded
		12	218	160	qz	subrounded
		13	117	64	diagenetic qz	doubly terminated
		14	69	53	qz	diagenetic
		15	80	74	qz	subangular
		16	69	48	qz	diagenetic
		17	96	69	qz	subangular
		18	85	80	qz	diagenetic
		19	101	59	qz	diagenetic
		20	85	53	qz	subangular
GH2	3	1	420	122	diagenetic qz	doubly terminated
		2	340	186	diagenetic qz	doubly terminated
		3	441	234	diagenetic qz	doubly terminated
		4	324	144	diagenetic qz	doubly terminated
		5	606	191	diagenetic qz	doubly terminated
		6	521	223	diagenetic qz	doubly terminated
		7	383	191	diagenetic qz	doubly terminated
		8	218	202	qz	diagenetic
		9	383	170	diagenetic qz	doubly terminated
		10	239	154	qz	diagenetic
		11	133	106	qz	rounded
		12	202	112	qz	diagenetic
		13	106	69	qz	diagenetic
		14	144	122	diagenetic qz	doubly terminated
		15	144	101	qz	diagenetic
		16	223	128	diagenetic qz	doubly terminated
		17	170	117	qz	diagenetic
		18	128	90	qz	diagenetic
		19	186	112	qz	diagenetic
		20	202	149	diagenetic qz	doubly terminated
GH2	3.3	1	761	415	diagenetic qz	doubly terminated
		2	894	543	qz	angular
		3	1069	830	diagenetic qz	doubly terminated
		4	633	415	qz	subangular

		5	426	362	qz	subangular
		6	431	335	qz	diagenetic
		7	590	202	diagenetic qz	doubly terminated
		8	553	176	diagenetic qz	doubly terminated
		9	293	223	qz	angular
		10	543	165	diagenetic qz	doubly terminated
		11	293	223	diagenetic qz	doubly terminated
		12	543	165	diagenetic qz	doubly terminated
		13	245	90	qz	angular
		14	298	106	diagenetic qz	doubly terminated
		15	149	64	qz	angular
		16	96	479	qz	angular
		17	261	176	qz	angular
		18	356	160	diagenetic qz	doubly terminated
		19	191	90	qz	diagenetic
		20	330	197	diagenetic qz	doubly terminated
GH2	3.6	1	335	282	diagenetic qz	Subrounded
		2	144	90	hematite	angular
		3	128	122	qz	subrounded
GH2	4	1	1064	559	qz	angular
		2	372	149	qz	angular
		3	478	266	qz	angular
		4	330	218	qz	subrounded
GH2	5	1	219	153	qz	subrounded
		2	255	177	qz	diagenetic
		3	115	77	qz	subrounded
		4	219	70	qz	diagenetic
		5	213	64	qz	diagenetic
		6	262	94	qz	diagenetic
		7	219	55	qz	diagenetic
		8	217	70	qz	diagenetic
		9	170	70	qz	diagenetic
		10	166	57	qz	diagenetic
		11	70	319	qz	diagenetic
		12	74	49	qz	angular
		13	106	43	qz	diagenetic
		14	64	43	qz	angular
		15	89	36	qz	diagenetic
		16	145	49	qz	diagenetic
		17	100	12.7	qz	diagenetic
		18	153	47	qz	diagenetic
		19	191	64	qz	diagenetic

		20	106	53	qz	diagenetic
GH2	5.2	1	564	266	diagenetic qz	doubly terminated
		2	426	293	diagenetic qz	doubly terminated
		3	973	543	clay	subangular
		4	484	372	diagenetic qz	doubly terminated
GH2	5.4	1	245	149	qz	diagenetic
		2	271	229	qz	subangular
		3	277	207	qz	subangular
		4	245	186	qz	diagenetic
		5	319	255	qz	diagenetic
		6	303	181	qz	subrounded
		7	261	170	qz	subrounded
		8	245	176	qz	diagenetic
		9	250	154	qz	diagenetic
		10	335	165	qz	angular
		11	122	96	K-spar	subrounded
		12	165	122	qz	angular
		13	133	85	qz	angular
		14	154	144	qz	angular
		15	160	90	qz	diagenetic
		16	138	90	qz	angular
		17	202	197	qz	diagenetic
		18	223	197	qz	subrounded
		19	277	186	qz	subrounded
		20	106	64	qz	angular
GH2	5.5	1	69	53	qz	subrounded
		2	133	64	qz	angular
		3	149	48	qz	angular
GH2	5.9	1	261	160	qz	diagenetic
		2	255	181	qz	diagenetic
		3	340	154	qz	diagnetic
		4	239	234	qz	angular
		5	239	207	qz	diagenetic
		6	165	149	qz	subrounded
		7	170	160	qz	subrounded
		8	218	213	qz	subrounded
		9	170	117	qz	subangular
		10	181	133	qz	diagenetic
		11	202	122	qz	subrounded
		12	213	176	qz	diagenetic
		13	128	96	qz	angular

		14	160	101	qz	diagenetic
		15	197	122	qz	diagenetic
		16	96	90	clay	angular
		17	160	90	qz	angular
		18	149	74	qz	subrounded
		19	117	96	qz	subrounded
		20	160	106	qz	subangular
GH2	6.7	1	324	213	qz	subrounded
		2	362	223	qz	subrounded
		3	346	154	qz	Diagenetic
		4	239	165	qz	Diagenetic
		5	282	197	qz	angular
		6	250	160	qz	Diagenetic
		7	234	133	qz	angular
		8	250	181	qz	Diagenetic
		9	266	128	qz	Diagenetic
		10	319	218	qz	diagenetic
		11	160	154	qz	subrounded
		12	149	117	qz	rounded
		13	165	144	qz	subangular
		14	202	128	qz	rounded
		15	239	160	qz	rounded
		16	101	69	qz	diagenetic
		17	128	69	qz	diagenetic
		18	223	149	qz	Diagenetic
		19	150	112	qz	subrounded
		20	128	85	qz	diagenetic
GH2	9.5	1	261	250	clay	subangular
		2	133	37	clay	angular
		3	160	53	clay	angular

Appendix 4

Table depicting Nd-Sr isotopic compositions of fine-grained extracted material (n=6) and large grains (n=3).

Nd-Sr isotopic compositions of fine-grained extracted material (n=6) and large grains (n = 3).

Sample	$^{87}Sr/^{86}Sr$ (meas)	±2SE (meas)	±2SE (%)	143Nd/144Nd	±2SE (meas)	εNd	±2SE
UHA-2.7	0.706916	0.000004	0.0006	0.512456	0.000003	-3.6	0.1
UHA-4.9*	0.705236	0.000005	0.0006	0.512692	0.000003	1.1	0.1
UHA-16.7*	0.705136	0.000004	0.0005	0.512684	0.000004	0.9	0.2
UHA-19.3	0.721968	0.000004	0.0005	0.512261	0.000010	-7.4	0.4
UHA-20.6	0.709214	0.000008	0.0012	0.512251	0.000004	-7.5	0.1
UHA-39.4*	0.705260	0.000009	0.0013	0.512690	0.000004	1.0	0.1
MNE-16.5	0.706405	0.000004	0.0006	0.512540	0.000004	-1.9	0.2
MNE-5.6-1G2	0.724348	0.000004	0.0006	0.512330	0.000004	-6.0	0.2
MNE-5.6-2G2	0.726455	0.000004	0.0006	0.512358	0.000017	-5.5	0.7
BCR-2 reference	0.705042	0.000005	0.0007	0.512629	0.000004	-0.2	0.1
certified value	**0.705000**			**0.512637**		**0.0**	

lithic fragment